PLOS ONE

Altered GC- and AT-biased genotypes of *Ophiocordyceps sinensis* in the stromal fertile portions and ascospores of natural *Cordyceps sinensis*

Yu-Ling Li[1¶], Ling Gao[2¶], Yi-Sang Yao[2¶], Xiu-Zhang Li[1], Zi-Mei Wu[3], Ning-Zhi Tan[2], Zhou-Qing Luo[3,#a], Wei-Dong Xie[2], Jian-Yong Wu[4,5], Jia-Shi Zhu[1,2]*

[1] State Key Laboratory of Plateau Ecology and Agriculture, Qinghai Academy of Animal and Veterinary Sciences, Qinghai University, Xining 810016, Qinghai, China

[2] Shenzhen Key Laboratory of Health Science and Technology, Institute of Biopharmaceutical and Health Engineering, Shenzhen International Graduate School, Tsinghua University, Shenzhen 518055, Guangdong, China

[3] School of Life Sciences, Tsinghua University, Beijing 100084, China

[4] State Key Laboratory of Chinese Medicine and Molecular Pharmacology, Shenzhen 518057, Guangdong, China

[5] Department of Applied Biology and Chemistry Technology, The Hong Kong Polytechnic University, Hong Kong

[#a] Current address: State Key Laboratory of Cellular Stress Biology, School of Life Sciences, Faculty of Medicine and Life Sciences, Xiamen University, Xiamen 361102, China

* Corresponding author

E-mail: zhujosh@163.com (JSZ)

[¶] These authors contributed equally to this work.

Short title:

Altered GC- and AT-biased genotypes of *Ophiocordyceps sinensis* in natural *Cordyceps sinensis*

Abstract:

Objective: To examine multiple genotypes of *Ophiocordyceps sinensis* in the stromal fertile portion (SFP) densely covered with numerous ascocarps and ascospores of natural *Cordyceps sinensis*. **Methods:** Mature *C. sinensis* specimens were harvested and continuously cultivated in our laboratory (altitude 2,200 m). The SFPs (with ascocarps) and fully and semi-ejected ascospores were collected for histological and molecular examinations. Biochip-based single nucleotide polymorphism (SNP) MALDI-TOF mass spectrometry (MS) was used to genotype multiple *O. sinensis* mutants in the SFPs and ascospores. **Results:** Microscopic analysis demonstrated distinct morphologies of the SFPs (with ascocarps) before and after ascospore ejection and the SFP of developmental failure, which, along with the fully and semi-ejected ascospores, were subjected to SNP MS genotyping analysis. Mass spectra showed the coexistence of GC- and AT-biased genotypes of *O. sinensis* that were genetically and phylogenetically distinct in the SFPs before and after ejection and of developmental failure and in fully and semi-ejected ascospores. The intensity ratios of MS peaks were dynamically altered in the SFPs and the fully and semi-ejected ascospores. Mass spectra also showed transversion mutation alleles of unknown sequences with altered intensities in the SFPs and ascospores. Genotype #5 of AT-biased Cluster-A maintained a high intensity in all SFPs and ascospores. An MS peak with a high intensity containing AT-biased Genotypes #6 and #15 in pre-ejection SFPs was significantly attenuated after ascospore ejection. The abundance of Genotypes #5–6 and #16 of AT-biased Cluster-A was differentially altered in the fully and semi-ejected ascospores that were collected from the same *C. sinensis* specimens. **Conclusion:** Multiple *O. sinensis* genotypes coexisted in different combinations with altered abundances in the SFPs prior to and after ejection, the SFP of developmental failure and in the two types of ascospores of *C. sinensis*, demonstrating their genomic independence. Fungal metagenomic members present in different combinations and with dynamic alterations play symbiotic roles in different compartments of natural *C. sinensis*.

Keywords: natural *Cordyceps sinensis*; stromal fertile portion; ascospores; MassARRAY single nucleotide polymorphism MALDI-TOF mass spectrometry genotyping; GC- and AT-biased genotypes of *Ophiocordyceps sinensis*; transition point mutation; transversion point mutation

Introduction

Natural *Cordyceps sinensis* is one of the most highly valued therapeutic agents in traditional Chinese medicine, with a centuries-long history of clinical use as a folk medicine administered for "Yin-Yang" double invigoration, health maintenance, disease amelioration, and post-disease and post-surgery recovery [1–2]. Modern pharmacological studies have validated the therapeutic profile and lifespan-extending properties of natural *C. sinensis* and its mycelial fermentation products [2–5]. The Chinese Pharmacopeia defines natural *C. sinensis* as an insect-fungal complex consisting of the *Ophiocordyceps sinensis* fruiting body and a dead Hepialidae moth larva, *i.e.*, natural *C. sinensis* ≠ *O. sinensis* fungus [6–10]. Studies have reported that the caterpillar body of *C. sinensis* contains an intact larval intestine, an intact and thick larval body wall with numerous bristles, head tissues, and fragments of other larval tissues [6–10]. Yao and Zhu [6] addressed the controversy surrounding the indiscriminate use of Latin names for natural insect-fungal complexes and multiple anamorphic-teleomorphic fungi. In this context, we temporarily refer to the fungus/fungi as *O. sinensis* in this paper and continue the customary use of the name *C. sinensis* to refer to the wild or cultivated insect-fungal complex, although this practice will likely be replaced by the discriminative use of exclusive Latin names for different biological entities in the future.

Natural *C. sinensis* grows only in alpine areas above 3,000–3,500 m on the Qinghai-Tibetan Plateau and has a complex lifecycle [2,7–10]. Its maturation stages greatly impact its compartmental mycobiota profile, metagenomic polymorphism and diversity, metatranscriptomic and proteomic expression, chemical constituent fingerprint, competitive proliferation of *Hirsutella sinensis*-like fungus/fungi, and therapeutic efficacy and potency as a natural therapeutic agent [7–25]. Mycologists have identified 22 species from 13 fungal genera in natural *C. sinensis* [26], and molecular methodologies have identified >90 species from >37 fungal genera and 17 genotypes of *O. sinensis* and demonstrated the predominance of different fungi and metagenomic fungal diversity in the stroma and caterpillar body of natural and cultivated *C. sinensis* [6–16,19–21,26–38].

Wei et al. [39] hypothesized that *H. sinensis* is the sole anamorph of *O. sinensis* based on the collection of 3 lines of evidence: (1) frequent isolation and mycological identification according to sporulation, conidial morphology and growth characteristics [26,40]; (2) microcycle conidiation of the ascospores [41–43]; and (3) systematic molecular analyses based on internal transcribed spacer (ITS) sequencing and random molecular marker polymorphism assays [28–32,39,44–45]. This hypothesis has been widely accepted because the evidence meets the first and second criteria of Koch's postulates. Wei

et al. [46] published a successful industrial artificial cultivation project reportedly using 3 GC-biased Genotype #1 *H. sinensis* strains as inoculants, seemingly satisfying the third criterion of Koch's postulates. However, they reported the detection of a single teleomorphic *O. sinensis* fungus in the fruiting body of cultivated *C. sinensis*, the sequence of which was reported to be identical to AT-biased Genotype #4 AB067749. Many studies have proven that the sequences of all AT-biased *O. sinensis* genotypes are not present in the genomes of 5 GC-biased Genotype #1 *H. sinensis* Strains Co18, 1229, CC1406-203, ZJB12195, and IOZ07 but instead belong to independent *O. sinensis* fungi [6–10,13,15–16,37,47–54]. Thus, the sequence mismatching between the inoculants and teleomorphic *O. sinensis* in cultivated *C. sinensis* products reported by Wei et al. [46] disproves the sole anamorph hypothesis for *H. sinensis* according to the fourth criterion of Koch's postulates.

Teleomorphs of *O. sinensis* found in natural *C. sinensis* specimens collected from different geographic areas have been reported to belong to Genotypes #1 [28,30,32,39], #3 [55–56], #4 [27,46], either #4 or #5 [29,57] and #7 [58] without coexisting with other genotypes of *O. sinensis*. Wei et al. [46] reported teleomorphs of GC-biased Genotype #1 and AT-biased Genotype #4 of *O. sinensis* in natural and cultivated *C. sinensis*, respectively. Li et al. [59] reported the detection of both GC-biased Genotype #1 and AT-biased Genotype #5 in 25-day cultures of teleomorphic monoascospores of natural *C. sinensis*. Bushley et al. [60] reported multicellular heterokaryotic mono-, bi-, and tri-nucleated structures of *C. sinensis* hyphae and ascospores. Li et al. [61 (the companion paper)] reported the differential coexistence of multiple GC- and AT-biased genotypes of *O. sinensis* in the stroma, stromal fertile portion (SFP) that was densely covered with numerous ascocarps, and ascospores of natural *C. sinensis*, which were altered dynamically during *C. sinensis* maturation. These findings regarding teleomorphic *O. sinensis* indicate that the independent metagenomic members of natural *C. sinensis* alternate dynamically and play symbiotic roles in different developmental and maturational stages of the *C. sinensis* lifecycle, constituting a natural integrated microecosystem [18].

In this study, we examined the microscopic morphology of SFPs prior to and after ascospore ejection and of developmental failure using the biochip-based MassARRAY single nucleotide polymorphism (SNP) MALDI-TOF mass spectrometry (MS) genotyping technique and examined the co-occurrence of GC- and AT-biased genotypes of *O. sinensis* in the SFPs and ascospores of natural *C. sinensis*. We observed differential co-occurrence and dynamic alterations of *O. sinensis* genotypes in a semiquantitative manner in the SFPs prior to and after ascospore ejection and of developmental failure and in the fully and semi-ejected ascospores of *C. sinensis*.

Materials and Methods

Reagents

Laboratory common reagents, such as ethanol, sucrose, paraformaldehyde, hematoxylin, eosin, agarose and electrophoresis reagents, were purchased from Beijing Bioland Technology Company. The Universal DNA Purification kit was a product of the TIANGEN Biotech Company, China. The DNeasy Plant Mini Kit was a product of Qiagen Company, Germany. The *Taq* PCR reagent kit and Vector NTI Advance 9 software were purchased from Invitrogen, United States. All reagents and biochips required for MassARRAY SNP MALDI-TOF MS genotyping were from Sequenom, USA, and experiments were performed at CapitalBio Co., Beijing.

Collection of *C. sinensis* specimens and *C. sinensis* SFPs and ascospores

C. sinensis specimens were purchased in local markets from the Hualong (located at 36°13'N, 102°19'E) and Yushu areas (located at 33°01'N, 96°48'E) of Qinghai Province, China (3800–4600 m altitude). Governmental permission was not required for *C. sinensis* purchases in local markets, and the collections of *C. sinensis* specimens from sales by local farmers fall under the governmental regulations for traditional Chinese herbal products.

Mature *C. sinensis* specimens were collected in mid-June. These specimens showed a plump caterpillar body and a long stroma (>5.0 cm) and the formation of an expanded fertile portion close to the stromal tip (*cf*. Fig 3A below), which was densely covered with ascocarps (*cf*. Fig 3B) [22,61].

Some of the mature *C. sinensis* specimens were harvested along with the outer mycelial cortices and soil surrounding the caterpillar body, replanted in paper cups in soil obtained from *C. sinensis* production areas and cultivated in our laboratory (altitude 2,200 m) in Xining City, Qinghai Province of China (*cf*. Fig 1 of the companion paper [61]). Because of the phototropism of natural *C. sinensis*, we kept the windows fully open, allowing sufficient sunshine and a natural plateau breeze blowing over the cultivated specimens in the paper cups. The room temperature was maintained naturally, fluctuating with the lowest

158 temperature at 18−19°C during the night and the highest temperature at 22−23°C in the early afternoon.
159 The humidity of our laboratory was maintained by spraying water using an atomizer twice a day in the
160 morning and evening [61].

161 Fig 1 of the companion paper [61] shows a collection of the fully ejected ascospores of *C. sinensis*
162 using double layers of autoclaved weighing paper. It also showed numerous ascospores adhered to the
163 outer surface of asci during massive ascospore ejection, which failed to be brushed off for collection using
164 an autoclaved brush; hence, these ascospores were instead gently scratched off using a disinfected
165 inoculation shovel or ring and referred to as semi-ejected ascospores.

166 The fully and semi-ejected ascospores were cleaned separately by 2 washes with 10% and 20%
167 sucrose solutions and 10-min centrifugation at 1,000 rpm (desktop centrifuge, Eppendorf, Germany); the
168 supernatant was discarded after each centrifugation. The pellets (ascospores) were subsequently washed
169 with 50% sucrose solution and centrifuged for 30 min, and the ascospores that floated on the liquid were
170 collected [61–62]. The 2 types of ascospores were stored in a -80°C freezer prior to further processing.

171 The SFPs (*cf.* Fig 3A below) were sampled prior to and after ascospore ejection and of developmental
172 failure that showed no sign of ascospore ejection during prolonged cultivation. These SFP samples were
173 stored in a -80°C freezer prior to further processing for DNA extraction.

174

175 Histological examination of the SFP, ascocarps and ascospores of *C.* 176 *sinensis*

177 Some of the mature *C. sinensis* stroma specimens collected prior to and after the massive ejection
178 of ascospores and of developmental failure were immersed in 10% formalin for fixation and subjected to
179 dehydration in 50%, 70% and 95% ethanol for 1 h each [63]. The SFP tissues (with numerous ascocarps)
180 were embedded in paraffin and sliced to 5-μm thickness (Model TN7000 Microtome, Tanner Scientific,
181 Germany) [61,63]. The ascus slices were stained with hematoxylin-eosin (HE) and observed under optical
182 and confocal microscopes (Model Primo Star and Model LSM780, ZEISS, Germany).

183

184 Sample preparation and extraction of genomic DNA

185 The frozen SFP samples were individually ground to a powder in liquid nitrogen, including the SFPs

186 (with ascocarps) (1) prior to ascospore ejection, (2) after ascospore ejection, and (3) of developmental
187 failure, each of which was a combination of 5 specimens. The ascospores (4) fully ejected and (5) semi-
188 ejected were collected from 5 *C. sinensis* specimens and treated in a lysate solution before extracting
189 genomic DNA [61]. Genomic DNA was individually extracted from these SFP powders and lysated
190 ascospores using the DNeasy Plant Mini Kit (Qiagen) according to the manufacturer's manual [14,22,61]
191 and quantified by measuring the absorbance at UV_{260} (Eppendorf BioSpectrometer®; Hamburg,
192 Germany).

193

194 Primer design for the first-step PCR in SNP genotyping analysis

195 The primers *Hsprp1*, *Hsprp3*, *ITS4*, *P1*, *P2* and *P4* were used in the first-step PCR (Table 1, Fig 1)
196 to amplify the ITS1-5.8S-ITS2 segments according to the following protocol: (1) 95°C for 5 min; (2) 35
197 cycles of 95°C for 30 s, 55°C for 30 s, and 72°C for 1 min; (3) 72°C for 10 min; with final holding at 4°C
198 [14,19–20]. The primer pairs *Hsprp1/3* and *Hsprp1/ITS4* were favorable for amplifying the ITS sequences
199 of GC-biased genotypes, and the primer pairs *P1/P2*, *P2/P1* and *P2/P4* were designed to amplify the
200 sequences of AT-biased genotypes. All primers were synthesized by Invitrogen Beijing Lab. or Beijing
201 Bomaide Technology Co. Amplicons from the first-step PCR were quantified by measuring the
202 absorbance at UV_{260} and examined by agarose gel electrophoresis.

203 **Table 1.** Universal primer and genotype-specific primers for the first-step PCR amplification of ITS segments.

Primer Name	**Direction**	**Primer sequence**
For amplification of the ITS sequences of GC-biased Genotype #1		
Hsprp1	Forward	ATTATCGAGTCACCACTCCCAAACCCCC
Hsprp3	Reverse	CGAGGTTCTCAGCGAGCTACT
ITS4	Reverse	TCCTCCGCTTATTGATATGC
For amplification of the ITS sequences of AT-biased genotypes		
P1 ($AB067740_{260–279}$, $AB067744_{256–275}$)	Forward	ACGCAGCGAAATACGATAAG
P2 ($AB067740_{356–338}$, $AB067744_{352–334}$)	Reverse	CATGCCCGCTAGAGTGCTA
P4 ($AB067740_{260–279}$, $AB067744_{256–267}$)	Forward	ACGCAGCGAAATGCAATAAG

204

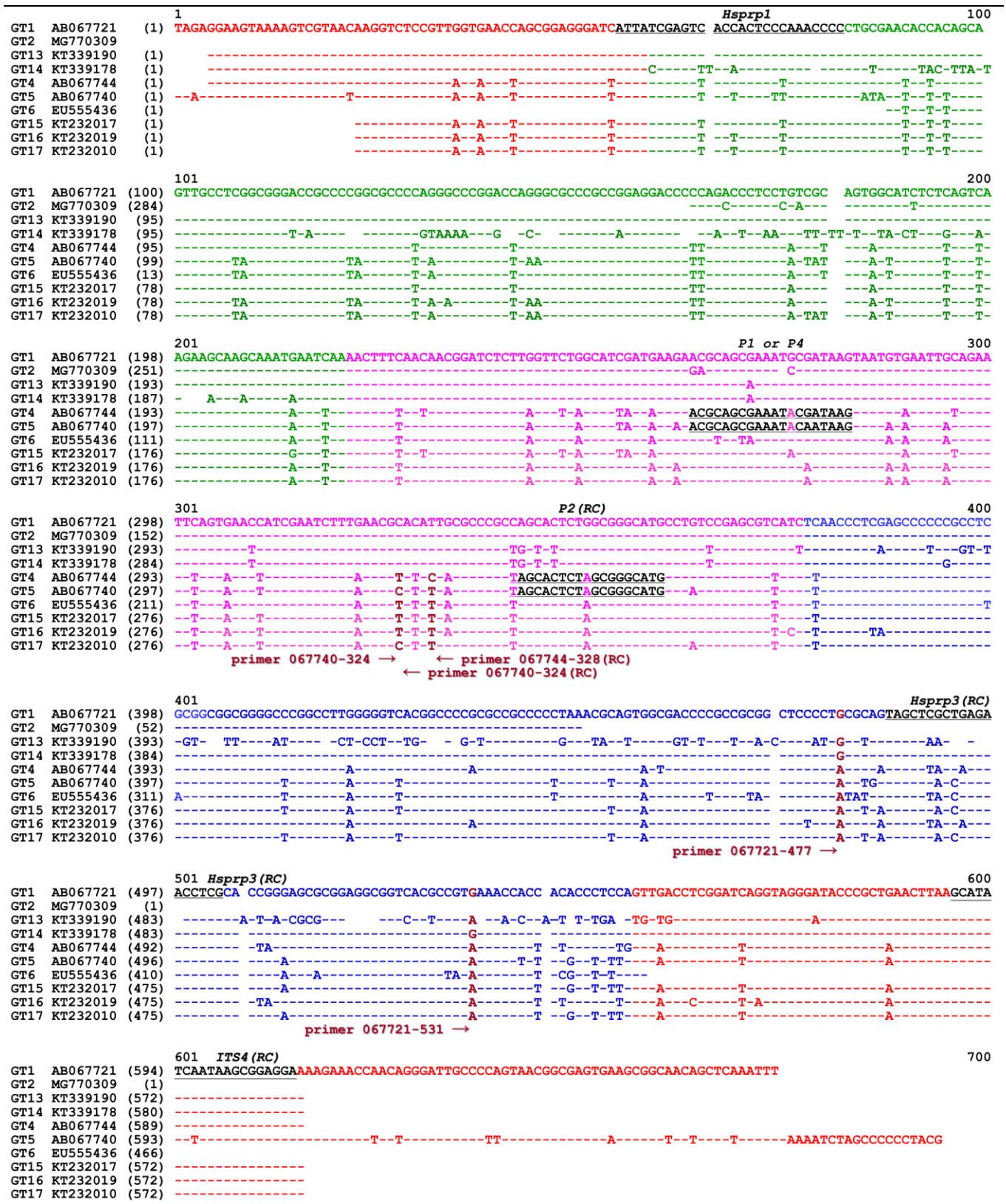

Fig 1. Alignment of ITS sequences of GC- and AT-biased genotypes of *O. sinensis* and primer locations. GT refers to genotype. Genotypes #1–3 and #13–14 are GC-biased *O. sinensis* genotypes, and Genotypes #4–6 and

#15–17 are AT-biased *O. sinensis* genotypes. The underlined sequences in black represent primers for the first-step PCR. Extension primers 067721-477, 067721-531, 067740-324, 067744-324 (RC, reverse complement) and 067740-328 (RC) in brown were used for SNP mass spectrometry genotyping to distinguish between genotypes of *O. sinensis*. Arrows indicate the directions of the primer extension reactions toward the SNP alleles in brown. "-" refers to an identical base, and spaces refer to unmatched sequence gaps.

Phylogenetic analysis of multiple genotypes of *O. sinensis*

Seventeen genotypes of *O. sinensis* available in GenBank were analyzed by conferring a phylogenetic tree using the maximum likelihood (ML) algorithm with MEGA software (Fig 2) [64] to assist in the design and analysis of the SNP genotyping experiment. The ITS sequences of 5 genomes of Genotype #1 *H. sinensis* Strains 1229, CC1406-203, Co18, IOZ07, and ZJB12195, either a single ITS copy or multiple repetitive ITS copies, were included in the phylogenetic analysis [47,51–54]. The topology of the ML tree was verified with Bayesian majority rule consensus trees [10,61,65–67], which was inferred using MrBayes v3.2.7 software (the Markov chain Monte Carlo [MCMC] algorithm) from $3x10^4$ samples, with a sampling frequency of 10^3 iterations after discarding the first 25% of samples from a total of $4x10^6$ iterations [66].

Extension primer design for MassARRAY SNP MS genotyping analysis based on the phylogenetic relationships of multiple genotypes of *O. sinensis*

In addition to the GC-biased genotype clade (side-noted in blue in Fig 2), the AT-biased genotype clade (side-noted in red) contains 2 AT-biased branches [10,61,67]: AT-biased Cluster-A consists of Genotypes #5–6 and #16–17, and AT-biased Cluster-B consists of Genotypes #4 and #15. The representative sequences of GC-biased Genotype #1 AB067721, Genotype #5 AB067740 within AT-biased Cluster-A, and Genotype #4 AB067744 within AT-biased Cluster-B were used as the reference sequences for designing SNP extension primers (Table 2) for biochip-based MassARRAY SNP MALDI-TOF mass spectrometry genotyping. Extension primers 067721-477 and 067721-531 were used to distinguish between the GC- and AT-biased genotypes but not between the multiple AT-biased genotypes (*cf*. Fig 1) [15,19–20]. Extension primers 067740-324, 067744-324 (reverse complement), and 067740-328 (reverse complement) were used to distinguish between the multiple AT-biased genotypes using a stratification genotyping strategy.

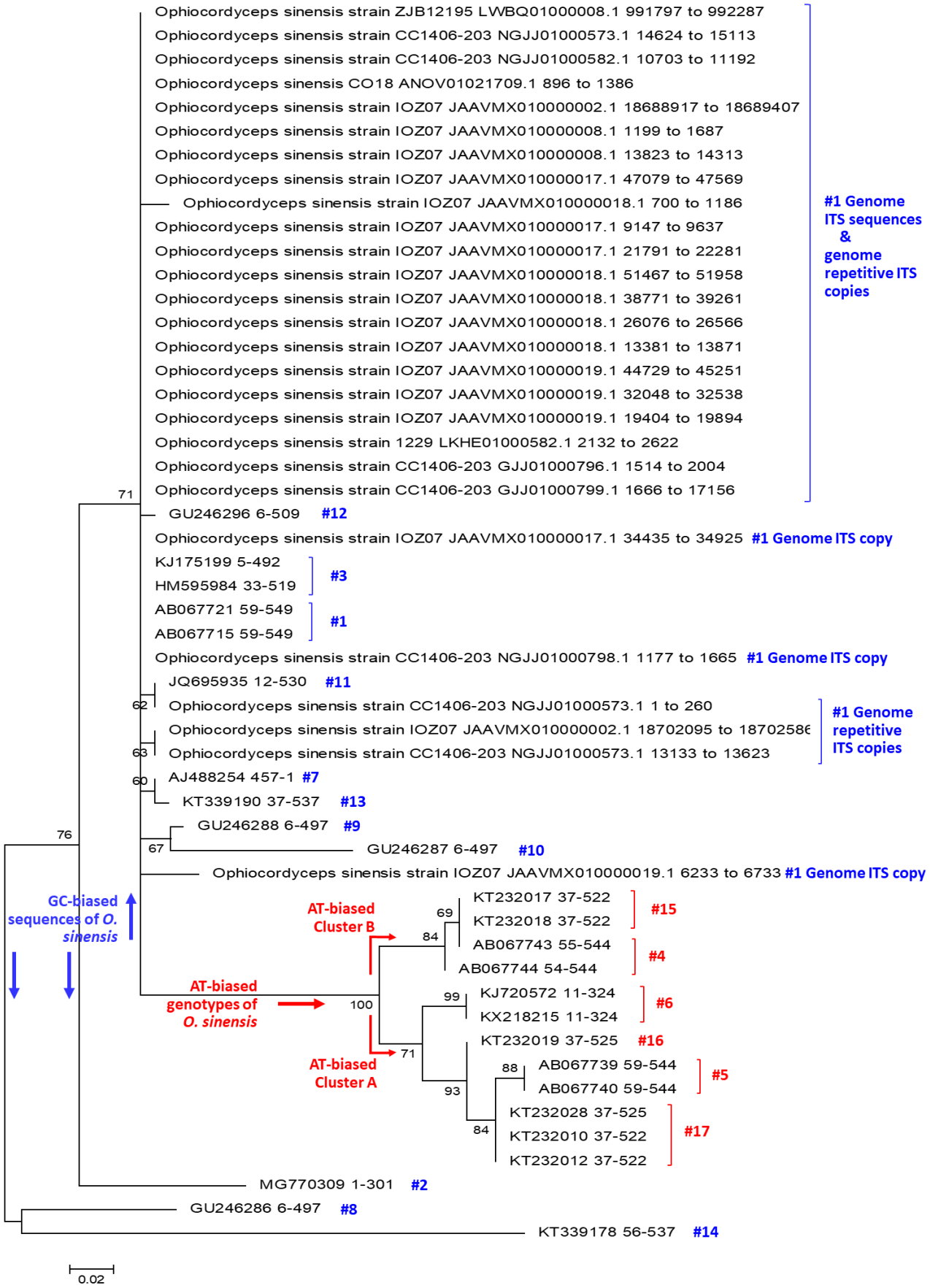
Ophiocordyceps sinensis strain ZJB12195 LWBQ01000008.1 991797 to 992287
Ophiocordyceps sinensis strain CC1406-203 NGJJ01000573.1 14624 to 15113
Ophiocordyceps sinensis strain CC1406-203 NGJJ01000582.1 10703 to 11192
Ophiocordyceps sinensis CO18 ANOV01021709.1 896 to 1386
Ophiocordyceps sinensis strain IOZ07 JAAVMX010000002.1 18688917 to 18689407
Ophiocordyceps sinensis strain IOZ07 JAAVMX010000008.1 1199 to 1687
Ophiocordyceps sinensis strain IOZ07 JAAVMX010000008.1 13823 to 14313
Ophiocordyceps sinensis strain IOZ07 JAAVMX010000017.1 47079 to 47569
Ophiocordyceps sinensis strain IOZ07 JAAVMX010000018.1 700 to 1186
Ophiocordyceps sinensis strain IOZ07 JAAVMX010000017.1 9147 to 9637
Ophiocordyceps sinensis strain IOZ07 JAAVMX010000017.1 21791 to 22281
Ophiocordyceps sinensis strain IOZ07 JAAVMX010000018.1 51467 to 51958
Ophiocordyceps sinensis strain IOZ07 JAAVMX010000018.1 38771 to 39261
Ophiocordyceps sinensis strain IOZ07 JAAVMX010000018.1 26076 to 26566
Ophiocordyceps sinensis strain IOZ07 JAAVMX010000018.1 13381 to 13871
Ophiocordyceps sinensis strain IOZ07 JAAVMX010000019.1 44729 to 45251
Ophiocordyceps sinensis strain IOZ07 JAAVMX010000019.1 32048 to 32538
Ophiocordyceps sinensis strain IOZ07 JAAVMX010000019.1 19404 to 19894
Ophiocordyceps sinensis strain 1229 LKHE01000582.1 2132 to 2622
Ophiocordyceps sinensis strain CC1406-203 GJJ01000796.1 1514 to 2004
Ophiocordyceps sinensis strain CC1406-203 GJJ01000799.1 1666 to 17156
#1 Genome ITS sequences & genome repetitive ITS copies
71
GU246296 6-509 #12
Ophiocordyceps sinensis strain IOZ07 JAAVMX010000017.1 34435 to 34925 #1 Genome ITS copy
KJ175199 5-492
HM595984 33-519
#3
AB067721 59-549
AB067715 59-549
#1
Ophiocordyceps sinensis strain CC1406-203 NGJJ01000798.1 1177 to 1665 #1 Genome ITS copy
JQ695935 12-530 #11
62
Ophiocordyceps sinensis strain CC1406-203 NGJJ01000573.1 1 to 260
Ophiocordyceps sinensis strain IOZ07 JAAVMX010000002.1 18702095 to 18702586
63
Ophiocordyceps sinensis strain CC1406-203 NGJJ01000573.1 13133 to 13623
#1 Genome repetitive ITS copies
60
AJ488254 457-1 #7
KT339190 37-537 #13
GU246288 6-497 #9
76
67
GU246287 6-497 #10
Ophiocordyceps sinensis strain IOZ07 JAAVMX010000019.1 6233 to 6733 #1 Genome ITS copy
GC-biased sequences of O. sinensis
AT-biased Cluster B
69
KT232017 37-522
KT232018 37-522
#15
84
AB067743 55-544
AB067744 54-544
#4
AT-biased genotypes of O. sinensis
100
99
KJ720572 11-324
KX218215 11-324
#6
KT232019 37-525 #16
71
AT-biased Cluster A
88
AB067739 59-544
AB067740 59-544
#5
93
84
KT232028 37-525
KT232010 37-522
KT232012 37-522
#17
MG770309 1-301 #2
GU246286 6-497 #8
KT339178 56-537 #14
0.02

238

Fig 2. A maximum likelihood (ML) phylogenetic tree. The ML tree was inferred using MEGA software [64], containing 25 ITS sequences (representing 17 genotypes of *O. sinensis*) and 27 genomic ITS sequences (including multiple repetitive ITS copies) of Genotype #1 *H. sinensis* Strain 1229, CC1406-203, Co18, IOZ07, and ZJB12195. The phylogenetic topology of the ML tree was verified according to the topologies of Bayesian majority-rule consensus phylogenetic trees [10,61,67].

Table 2. SNP extension primers for MassARRAY MALDI-TOF MS genotyping.

Primer Name	**Primer sequence**
Used in the second-step PCR designed based on the AB067721 sequence to amplify the GC-biased sequences of *O. sinensis* genotypes	
067721-477	CGCCGCGGCTCCCCT
067721-531	AGGCGGTCACGCCGT
Used in the second-step PCR designed based on both AB067744 and AB067740 sequences to amplify the AT-biased sequences of *O. sinensis* genotypes	
067740-324	GTAAACTATCGAATCTTTAAACG
067744-324 (reverse compliment)	GCTAGCGGGCGTAGTAT
067740-328 (reverse compliment)	GTGCTAGCGGGCGTA

Biochip-based MassARRAY SNP MALDI-TOF MS genotyping

ITS sequences were amplified using the aforementioned primer pairs from genomic DNA prepared from SFPs prior to and after ejection and of developmental failure and fully and semi-ejected ascospores. The amplicons obtained from the first-step PCR were subjected to neutralization of the unincorporated dNTPs with shrimp alkaline phosphatase and used as templates for single nucleotide extension toward the selected SNP sites shown in Fig 1. These amplicons were mixed with an iLEX Gold cocktail (Sequenom) containing one of the extension primers listed in Table 2 per reaction and amplified according to the following protocol: (1) 94°C for 30 s; (2) 94°C for 5 s; (3) 52°C for 5 s; (4) 80°C for 5 s; (5) return to (3) for 4 more times (for a total of 5 “smaller” cycles); (6) return to (2) for 39 more times (for a total of 40 “larger” cycles); (7) 72°C for 3 min; and (8) 4°C indefinitely [15,19–20]. After purification, the extended products with one of the mass-modified nucleotides were analyzed using SpectroCHIP (SEQUENOM), and their masses were analyzed using MALDI-TOF MS to determine heterogeneous genotypes [15,19–20,68]. The biochip-based MassARRAY SNP MALDI-TOF MS genotyping experiments were performed by CapitalBio Co. in Beijing, China.

Results

Microscopy observations of histological structures of the SFPs

Fig 3A shows a mature *C. sinensis* specimen labeled for the SFP (the stromal fertile portion), and Fig 3B shows a confocal image (bar: 1 mm) of a transverse section of the *C. sinensis* SFP, which is densely covered by numerous ascocarps. Fig 3C shows an optical microscopy image (40x) of an HE-stained *C. sinensis* ascocarp containing multiple ascospores prior to ejection. Fig 3D shows a confocal image (bar: 100 μm) of 2 ascocarps; the upper ascocarp is a maturing ascocarp with not yet opened perithecium containing multiple ascospores prior to ejection, and the lower ascocarp is a mature ascocarp during ascospore ejection with multiple ascospores aggregating toward the opening of the perithecium. Fig 3E shows a confocal image close to the opening of the perithecium during ascospore ejection with an arrow pointing to a semi-ejected ascospore hanging out of the opening of the perithecium. Fig 3F shows an optical microscopy image (10x) of HE-stained SFP after ascospore ejection. Panels 3G (10x) and 3H (40x) show optical images of HE-stained SFPs of developmental failure with abnormal structures of ascocarps (compared to normal structures shown in Figs 3C–3D) and containing no normally developed ascospores.

In addition, the lower-left panel of Fig 1 and Fig 3 of the companion paper [61] show the numerous semi-ejected ascospores that tightly adhered to the outer surface of asci and the microscopic images of fully ejected *C. sinensis* ascospores with or without calmodulin fluorescent staining, respectively.

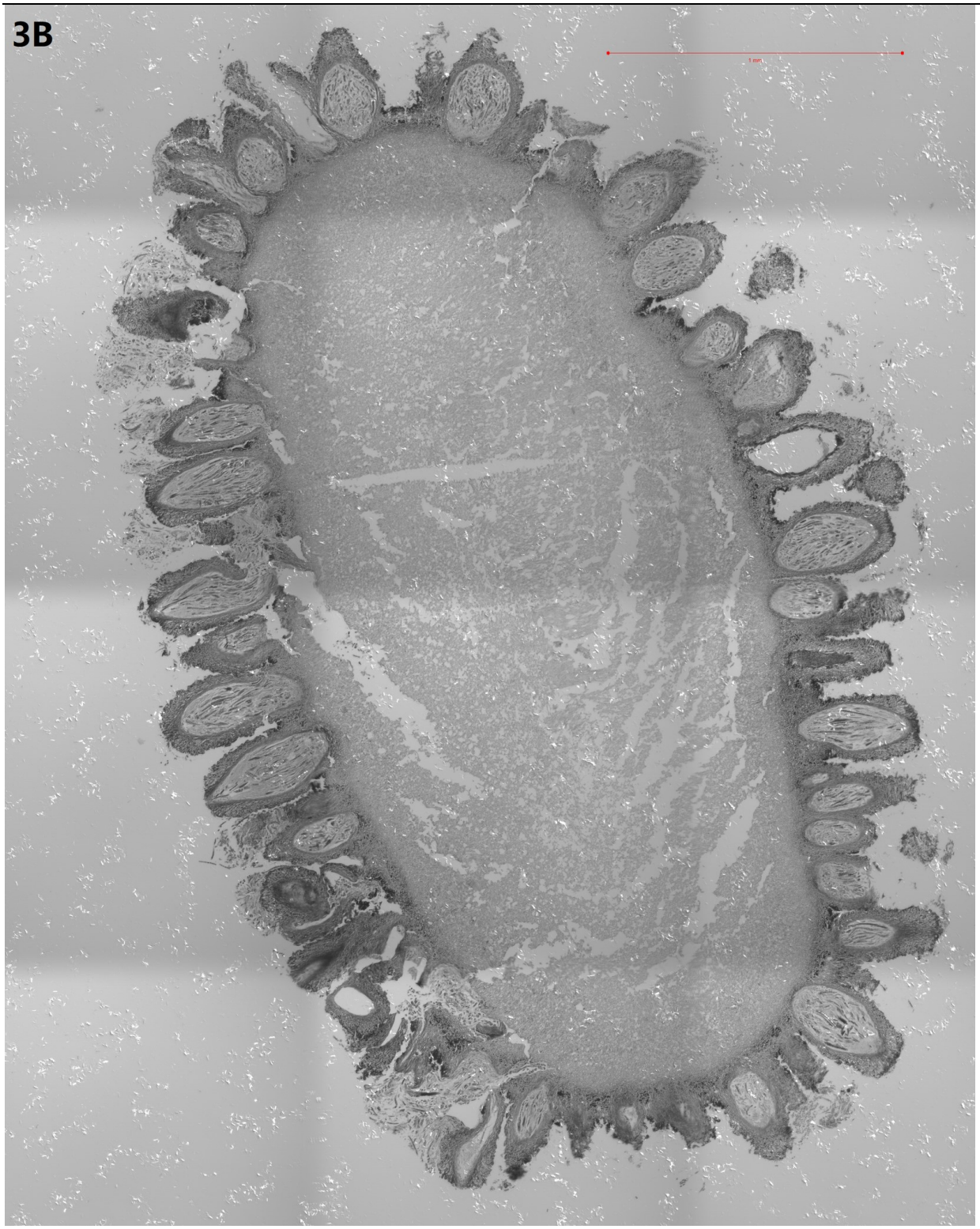

281

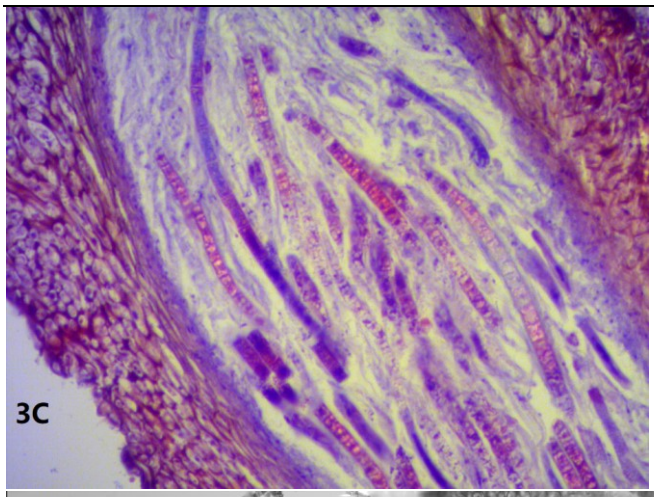
3C

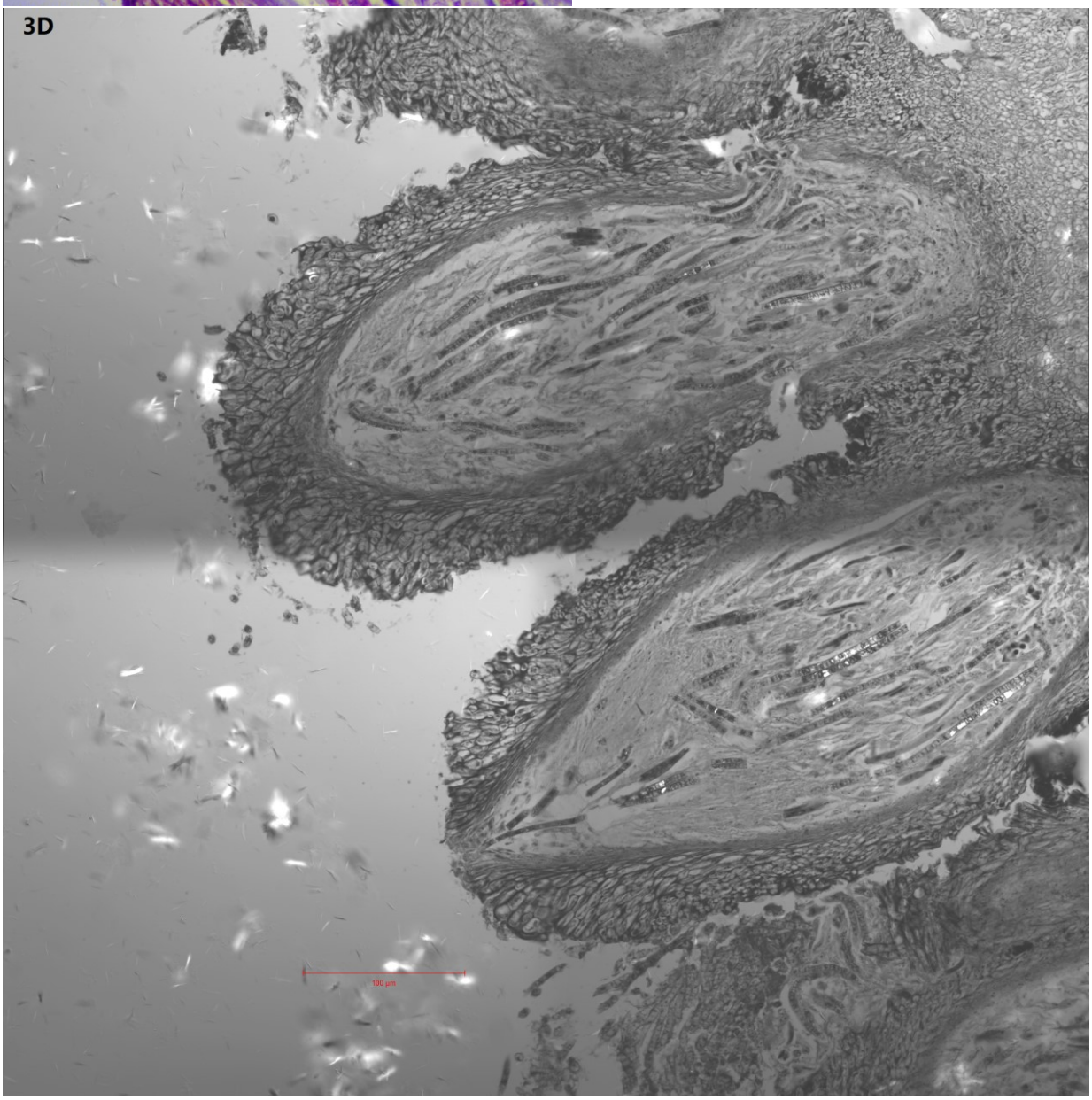
3D
100 µm

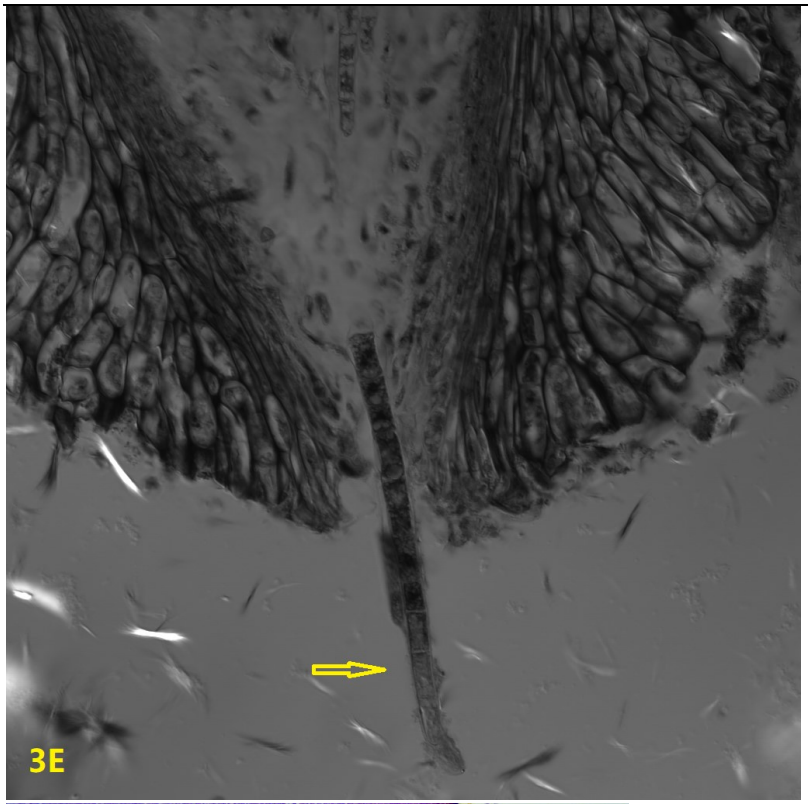
3E

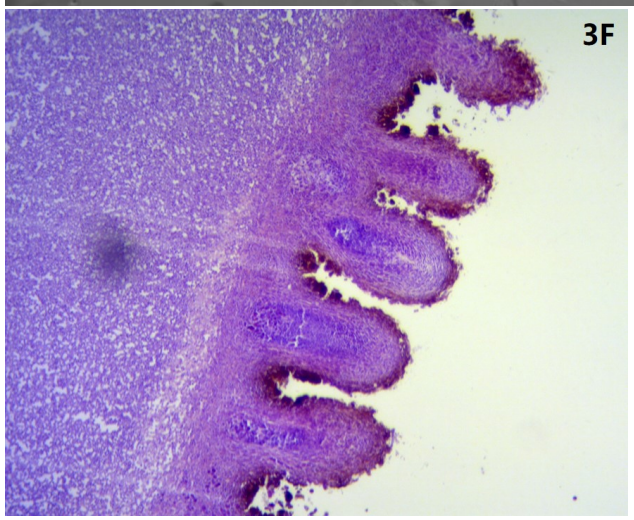
3F

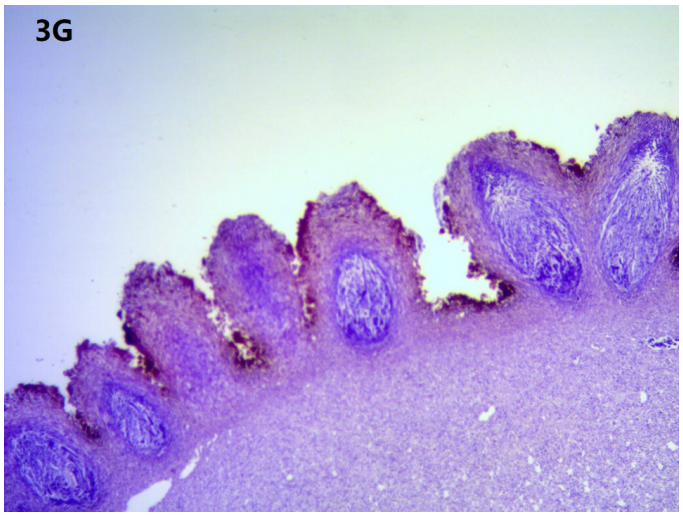
3G

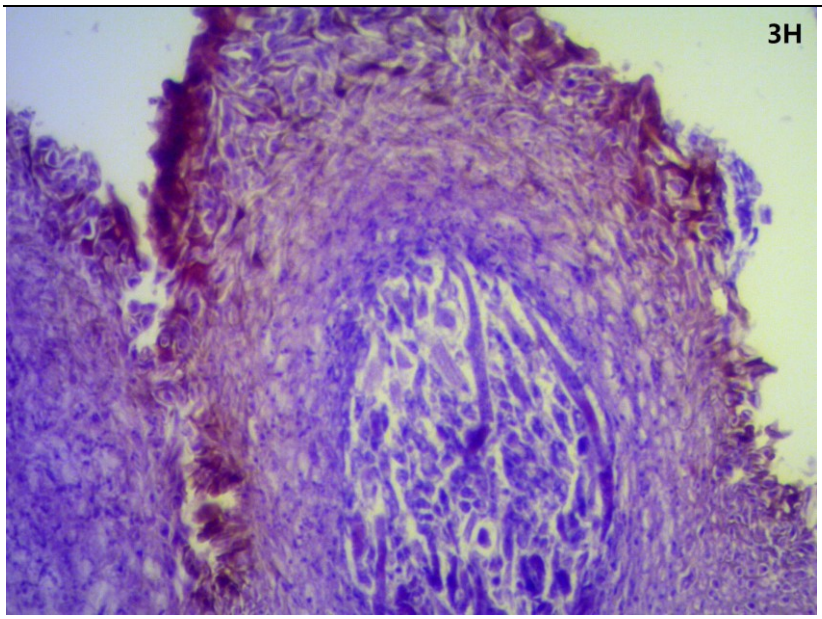

Fig 3. Microscopic images of the SFPs (with ascocarps) of natural *C. sinensis*. Panel 3A shows a photo of a mature *C. sinensis* specimen labeled with SFP (stromal fertile portion). Panel 3B shows a confocal image (bar: 1 mm) of a transverse section of the *C. sinensis* SFP prior to ascospore ejection. Panel 3C shows an optical close-up image (40x) of an HE-stained ascocarp containing multiple ascospores of multicellular ascosporic cells. Panel 3D shows a confocal image (bar: 100 μm) of 2 ascocarps; the upper one is a maturing ascocarp, and the lower one is a mature ascocarp containing multiple ascospores aggregating toward the opening of the perithecium. Panel 3E shows a confocal image close to the opening of the perithecium and a semi-ejected ascospore hanging out of the opening of the perithecium. Panel 3F shows an optical image (10x) of HE-stained SFPs after ascospore ejection. Panels 3G (10x) and 3H (40x) show optical images of HE-stained SFPs of developmental failure.

Phylogenetic analysis of 17 genotypes of *O. sinensis* and multiple repetitive ITS copies in the genome of Genotype #1 *H. sinensis*

The ML phylogenetic tree shown in Fig 2 shows the phylogeny of the 17 GC- and AT-biased genotypes of *O. sinensis* and the genome ITS sequences of Genotype #1 *H. sinensis*, including multiple repetitive ITS copies in the genome assemblies JAAVMX000000000 and NGJJ00000000 and a single copy each in ANOV00000000, LKHE00000000 and LWBQ00000000 of Genotype #1 *H. sinensis* Strains IOZ07, CC1406-203, Co18, 1229 and ZJB12195, respectively [47,51–54]. Notably, each of the genome assemblies ANOV00000000, LKHE00000000 and LWBQ00000000 of *H. sinensis* Strains Co18, 1229 and ZJB12195, respectively [47,52,54], contains only one ITS copy, indicating that other repetitive ITS copies might have been discarded during assembly of genome shotgun sequences. All these genomic ITS

307 sequences are GC biases and were clustered in the GC clade along with the GC-biased genotypes but far
308 distant from the AT-biased clade. The genome repetitive ITS copies contain none, less or more multiple
309 scattered insertion/deletion and transversion point mutations (will be analyzed in detail in a separate
310 paper). All AT-biased genotypes feature multiple scattered transition point mutations (*cf*. Fig 1), among
311 which Genotypes #5–6 and #16–17 are in AT-biased Cluster-A and Genotypes #4 and #15 in AT-biased
312 Cluster-B (*cf*. Fig 2). The genome assemblies of GC-biased Genotype #1 *H. sinensis* strains do not contain
313 any AT-biased genotype sequences, indicating genomic independence of the *O. sinensis* genotypes.
314

315 SNP genotyping to distinguish between GC- and AT-biased *O. sinensis* 316 genotypes in SFPs before and after ascospore ejection and of 317 developmental failure

318 Li et al. [61] reported the co-occurrence of GC-biased Genotype #1 *H. sinensis* and AT-biased
319 Genotypes #4–6 and #15 of *O. sinensis* in SFPs based on the application of several pairs of genotype-
320 specific primers and cloning-based amplicon sequencing approaches. The biochip-based MassARRAY
321 SNP MS genotyping technique was used to examine the dynamic alterations of the *O. sinensis* genotypes
322 in SFPs prior to and after ascospore ejection and of developmental failure in a semiquantitative manner.
323 Equal amounts of genomic DNA (calculated based on the absorbance at UV_{260}) were applied to the first-
324 step PCR using the primer pairs *Hsprp1/3* and *Hsprp1/ITS4* to amplify the ITS sequences of GC-biased
325 genotypes in greater quantities than those of AT-biased genotypes or the primer pairs *P1/P2*, *P2/P1* and
326 *P2/P4* to amplify the sequences of AT-biased genotypes (*cf*. Table 1 and Fig 1).
327 Extension primers 067721-477 and 067721-531 (*cf*. Table 2) were used in the second-step PCR, and
328 the reactions extended the extension primers with a single nucleotide toward the SNPs at positions 477
329 and 531 in the AB067721 sequence (*cf*. Fig 1). Mass spectra showed 4 allelic peaks, Peaks A, C, G, and
330 T representing the extension reactions of the primers 067721-477 and 067721-531 with a single extended
331 nucleotide adenine, cytosine, guanine, and thymine, respectively.
332

333 ## SNP genotyping using extension primer 067721-477

334 Fig 4A shows a mass spectrum of extension primer 067721-447 (*cf*. Table 2) for the SFP prior to
335 ascospore ejection. Peak G with the highest intensity represents the GC-biased Genotype #1 *H. sinensis*.
336 Peaks C, A, and T presented much lower intensities. Peak A represents AT-biased genotypes with transition
337 point mutations (*cf*. Fig 1), and Peaks C and T represent 2 transversion point mutation genotypes of
338 unknown sequences. The primers employed for the first-step PCR preferentially amplified GC-biased
339 genotype sequences, resulting in a greater quantity of GC-biased amplicons that served as the templates
340 for the second-step PCR. Table 3 shows the intensity ratios of the MS peaks: G:A, G:C and G:T.

341 Fig 4B shows a mass spectrum for the postejection SFP. The intensities of Peaks A and G appeared
342 to increase proportionally compared with the corresponding peaks shown in Fig 4A, resulting in a similar
343 G:A ratio (Table 3). In contrast, Peaks C and T were greatly attenuated, resulting in significant elevations
344 in the intensity ratios of G:C and G:T (Table 3). The ejection-related increase in the GC- and AT-biased
345 genotypes of *O. sinensis*, coupled with declines in the 2 unknown transversion mutation genotypes,
346 indicate that these genotypes play different roles in SFPs prior to, during and after ascospore ejection.

347 Fig 4C shows a mass spectrum for the SFP of developmental failure. Compared with Peaks G and A
348 shown in Fig 4A, the intensity of Peak G in Fig 4C was elevated, while Peak A remained unchanged,
349 resulting in a small elevation of the G:A intensity ratio (Table 3). Peak C was absent, while Peak T of the
350 transversion point mutation genotype was lower than that for the pre-ejection SFP shown in Fig 4A,
351 resulting in a significant elevation of the G:T ratio (Table 3).

352 Fig 4D shows the overlapping mass spectra of Figs 4A and 4B after adjusting and aligning the vertical
353 axis for intensity and visualizes the dynamic alteration of the allelic peaks in the SFPs from pre-ejection
354 to post-ejection.

355

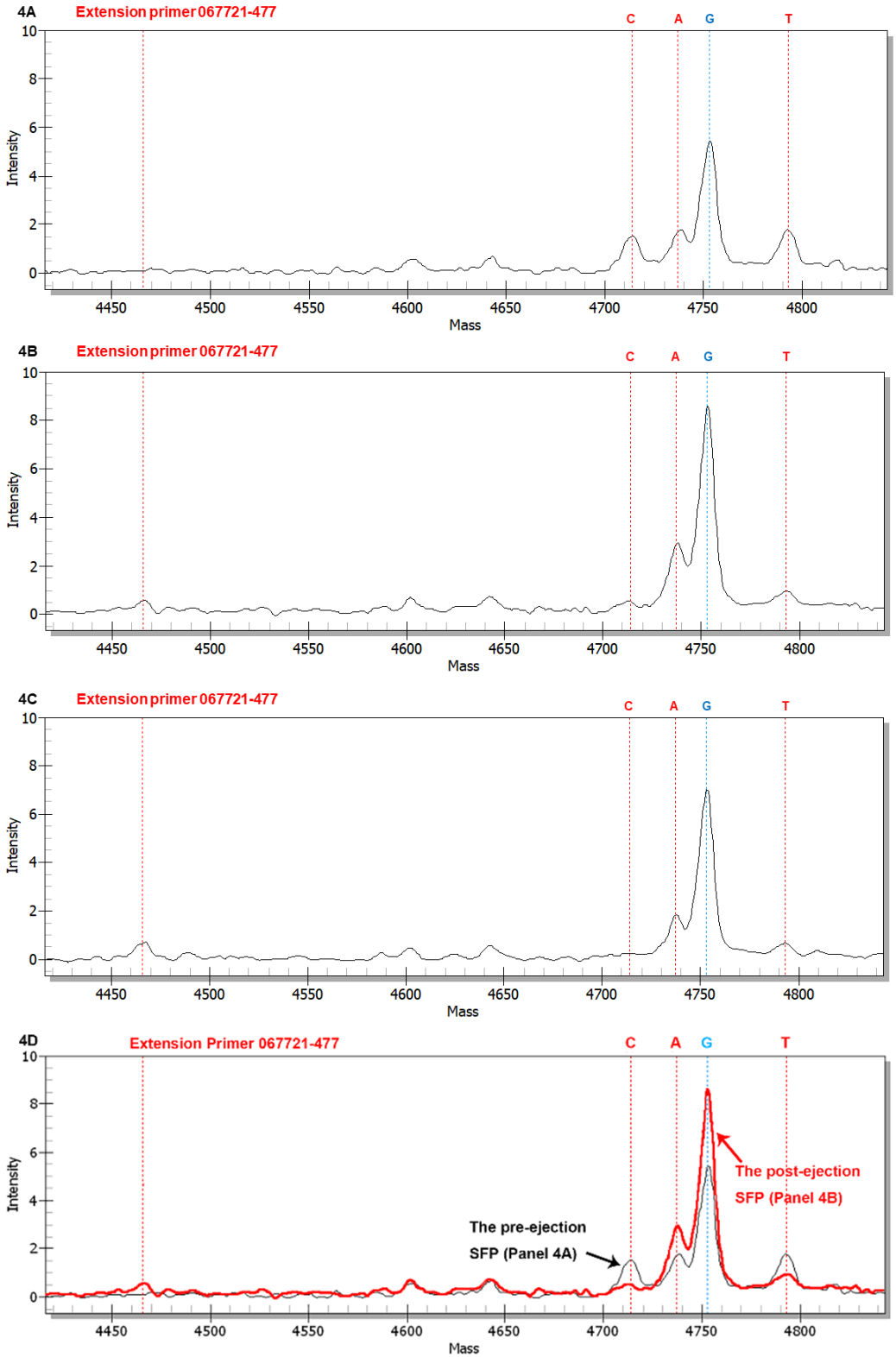

Fig 4. MALDI-TOF mass spectra (MS) of extension primer 067721-477 to distinguish between GC- and AT-genotypes in the SFPs (with ascocarps) prior to and after ascospore ejection and developmental failure. The extension reaction proceeded from extension primer 067721-477 toward the SNP at position 477 in the

AB067721 sequence (Fig 1 for the location). In the allelic peaks, "C" denotes extension of the primer with an extended cytosine; "A" indicates an extended adenine, "G" represents an extended guanine, and "T" refers to an extended thymine. Panel 4A shows the mass spectrum for the pre-ejection SFP. Panel 4B shows the mass spectrum for the postejection SFP. Panel 4C shows the mass spectrum for the SFP of developmental failure. Panel 4D shows the overlapping mass spectra for Panels 4A (black tracing) and 4B (red tracing) with alignment of the horizontal and vertical axes of the panels.

Table 3. Mass intensity ratios of the SNP peaks of transition and transversion mutation genotypes in the SFPs prior to and after ascospore ejection and of developmental failure.

Extension primer	**Allelic ratio**	**Intensity ratio**		
		Prior-ejection SFP (*cf.* Fig 4A)	**Post-ejection SFP** (*cf.* Fig 4B)	**SFP of developmental failure** (*cf.* Fig 4C)
067721-477	G:A	**3.3** (5.3÷1.6)	**3.0** (↔; 8.4÷2.8)	**3.9** (↑; 7.0÷1.8)
	G:C	**4.4** (5.3÷1.2)	**21.0** (↑↑↑↑; 8.4÷0.4)	—
	G:T	**3.3** (5.3÷1.6)	**9.3** (↑↑; 8.4÷0.9)	**10.0** (↑↑↑; 7.0÷0.7)

Note: Peak G represents GC-biased Genotype #1 *H. sinensis*; Peak A indicates AT-biased genotypes of *O. sinensis* (Fig 1). Peaks C and T denote 2 transversion mutation genotypes of unknown sequences. "↔" indicates no significant change (within 20% variation), and "↑" (increase not greater than 2 times), "↑↑" (increase between 2–3 times), "↑↑↑" (increase between 3–4 times) and "↑↑↑↑" (increase greater than 4 times) denote significant increases in intensity ratios compared to that in the pre-ejection SFP. "—" means that one of the allelic peaks was missing, and no ratio could be calculated.

SNP genotyping using extension primer 067721-531

Fig 5A shows a mass spectrum of extension primer 067721-531 (*cf.* Table 2) for the pre-ejection SFP, displaying allelic Peaks A and G with comparable intensities and resulting in a G:A intensity ratio of 1.06 (Table 4). Because the primers employed for the first-step PCR preferentially amplified the sequences of GC-biased genotypes, the comparable intensities of Peaks A and G might indicate a greater quantity of natural abundance of AT-biased genotypes than GC-biased Genotype #1 *H. sinensis* in the genomic DNA pool extracted from the pre-ejection SFP. While Peak C was absent, Peak T showed a very low intensity, representing a transversion mutation genotype of unknown sequences and resulting in a high G:T ratio of 12.7 (Table 4).

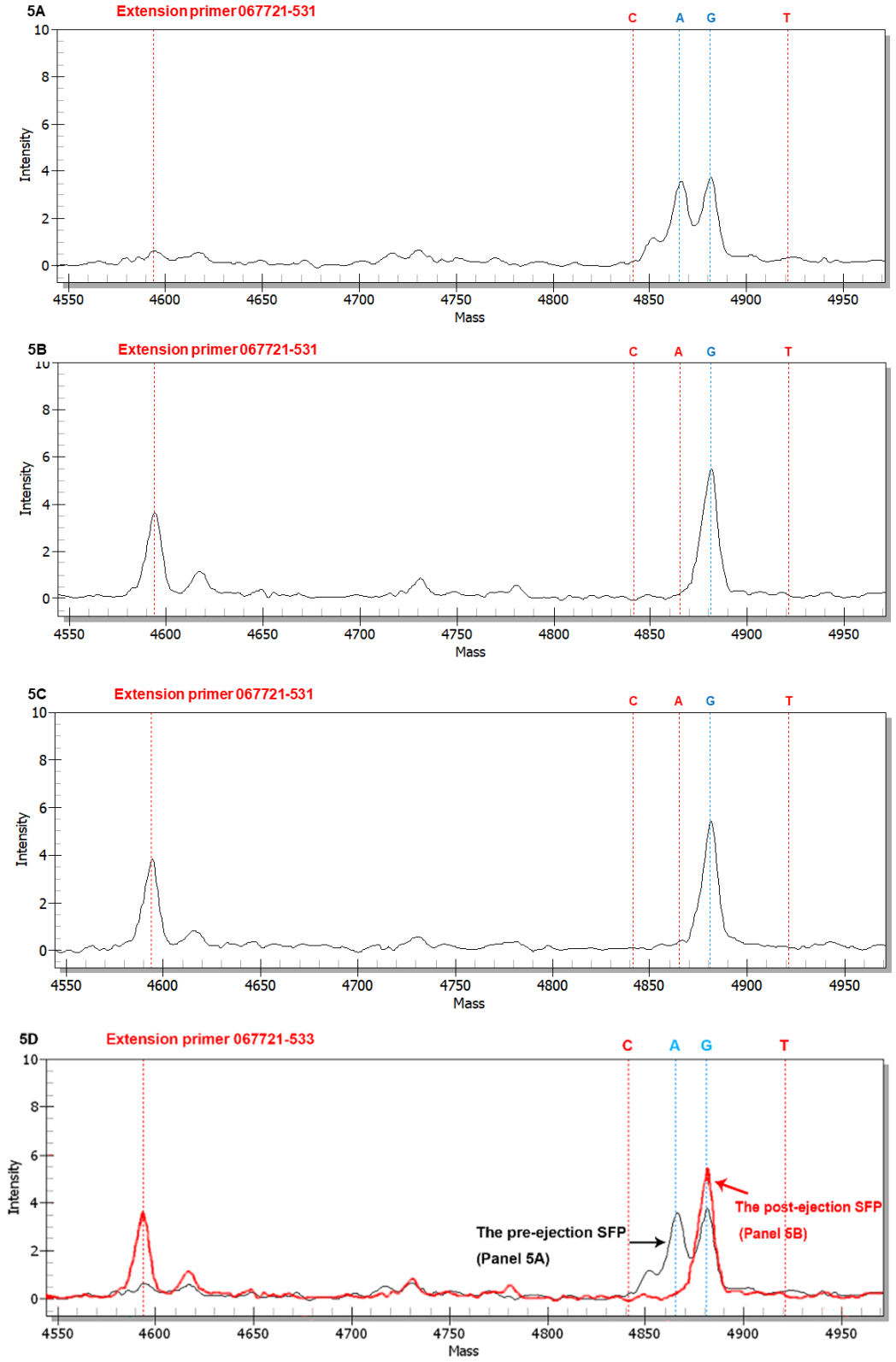

Fig 5. MALDI-TOF mass spectra (MS) of extension primer 067721-531 to distinguish between the GC- and AT-genotypes in the SFPs (with ascocarps) before and after ascospore ejection and the SFP that failed to develop and eject the ascospores. The extension primer 067721-531 was extended to the SNP at position 531 in

the AB067721 sequence (*cf.* Fig 1 for the location). The allele peaks are marked: "C" denotes the primer with an extended cytosine; "A" indicates an extended adenine, "G" represents an extended guanine, and "T" refers to an extended thymine. Panel 5A shows the mass spectrum for the SFP before ascospore ejection. Panel 5B shows the mass spectrum for the SFP after ascospore ejection. Panel 5C shows the mass spectrum for the SFP that failed to develop and eject the ascospore. Panel 5D shows the overlapping mass spectra for Panels 5A (black tracing) and 5B (red tracing) with alignment of the horizontal and vertical axes of the panels.

Table 4. Mass intensity ratios of the SNP peaks of transition and transversion mutation genotypes in the SFPs prior to and after ascospore ejection and of developmental failure.

Extension primer	**Allelic ratio**	**Intensity ratio**		
		Prior-ejection SFP (*cf.* Fig 5A)	**Post-ejection SFP** (*cf.* Fig 5B)	**SFP of developmental failure** (*cf.* Fig 5C)
067721-531	G:A	**1.06** (3.8÷3.6)	**19.3** (↑↑↑↑; 5.5÷0.3)	**13.5** (↑↑↑↑; 5.4÷0.4)
	G:C	—	—	—
	G:T	**12.7** (3.8÷0.3)	—	—

Note: Peak G represents GC-biased Genotype #1 *H. sinensis*; Peak A indicates AT-biased genotypes of *O. sinensis* (Fig 1). Peaks C and T denote 2 transversion mutation genotypes of unknown sequences. "↔" indicates no significant change, and "↑↑↑↑"denotes significant increases greater than 4 times in intensity ratios compared to that in the pre-ejection SFP. "—" means that one of the allelic peaks was missing and no ratio could be calculated.

Figs 5B and 5C show the mass spectra with similar topologies for the SFPs after ascospore ejection and of developmental failure, respectively, displaying an elevated Peak G and a considerably attenuated Peak A relative to those shown in Fig 5A. These results indicated significant decreases in the amount of AT-biased genotypes of *O. sinensis* in the SFPs after ascospore ejection and of developmental failure, while GC-biased Genotype #1 *H. sinensis* was relatively increased. The dynamic changes resulted in increases in the G:A intensity ratios to 19.3 and 13.5 for the SFPs after ejection and of developmental failure, respectively (Table 4), compared with a G:A ratio of 1.06 obtained for the pre-ejection SFP. Peaks C and T are absent in Figs 5B and 5C.

Fig 5D shows the overlapping mass spectra of Figs 5A and 5B after adjusting and aligning the vertical axis for intensity and visualizes the dynamic alteration of the allelic peaks in the SFPs from pre-ejection to post-ejection.

Stratified SNP genotyping to distinguish between the AT-biased genotypes of *O. sinensis* in the SFPs prior to and after ascospore ejection and of developmental failure

415 Li et al. [61] reported the detection of Genotypes #5–6 of AT-biased Cluster-A and Genotypes #4 and
416 #15 of Cluster-B in the SFP (*cf*. Fig 2). According to the sequence alignment shown in Fig 1, SNP MS
417 genotyping was performed *via* a stratification strategy using extension primers 067740-324, 067744-324
418 (reverse complement) and 067740-328 (reverse complement) (*cf*. Table 2) to distinguish between
419 Genotypes #4–6 and #15. The templates of the extension reactions were the amplicons obtained from the
420 first-step PCR using primer pairs *P1/P2*, *P2/P1* and *P2/P4* (*cf*. Table 1), which amplify the AT-biased
421 sequences of *O. sinensis*.

422

423 Using extension primer 067740-328 to distinguish between AT-biased Genotype #4 424 and other AT-biased genotypes

425 Fig 6A shows a mass spectrum of extension primer 067740-328 (reverse complement; *cf*. Fig 1 and
426 Table 2) for the SFP prior to ascospore ejection. Peak T was the major allele, representing the sum of the
427 mass intensities of Genotypes #5–6 and #15. Although the extension reaction using primer 067740-328
428 could also produce an extended thymine on the DNA templates of Genotypes #16–17 (*cf*. Fig 1), these
429 genotypes were absent in the SFPs of natural *C. sinensis* according to the results obtained using genotype-
430 specific primers and PCR amplicon-cloning techniques [61]. Peak C was buried in a descending MS loop,
431 representing a very low level of Genotype #4 (*cf*. Fig 1), resulting in a T:C intensity ratio of 14.1 (Table
432 5). Peak G was nearly flat and negligible. Peak A with a low intensity represented a co-occurring
433 transversion mutation genotype of an unknown sequence, resulting in a T:A ratio of 11.1 (Table 5).

434 Figs 6B and 6C show mass spectra for the SFPs after ascospore ejection and of developmental failure
435 with similar MS topologies. Compared with that shown in Fig 6A, Peak T (Genotypes #5–6 and #15)
436 remained the major allele with increased intensities in both Figs 6B and 6C. Peak C (Genotype #4) was
437 still buried in the descending loop, resulting in a similar (Fig 6B) or an increased (Fig 6C) T:C ratio (Table
438 5). Peak A (a transversion point mutation genotype of an unknown sequence) was attenuated in Figs 6B–
439 6C relative to that shown in Fig 6A, resulting in increases in the T:A ratio (Table 5).

440

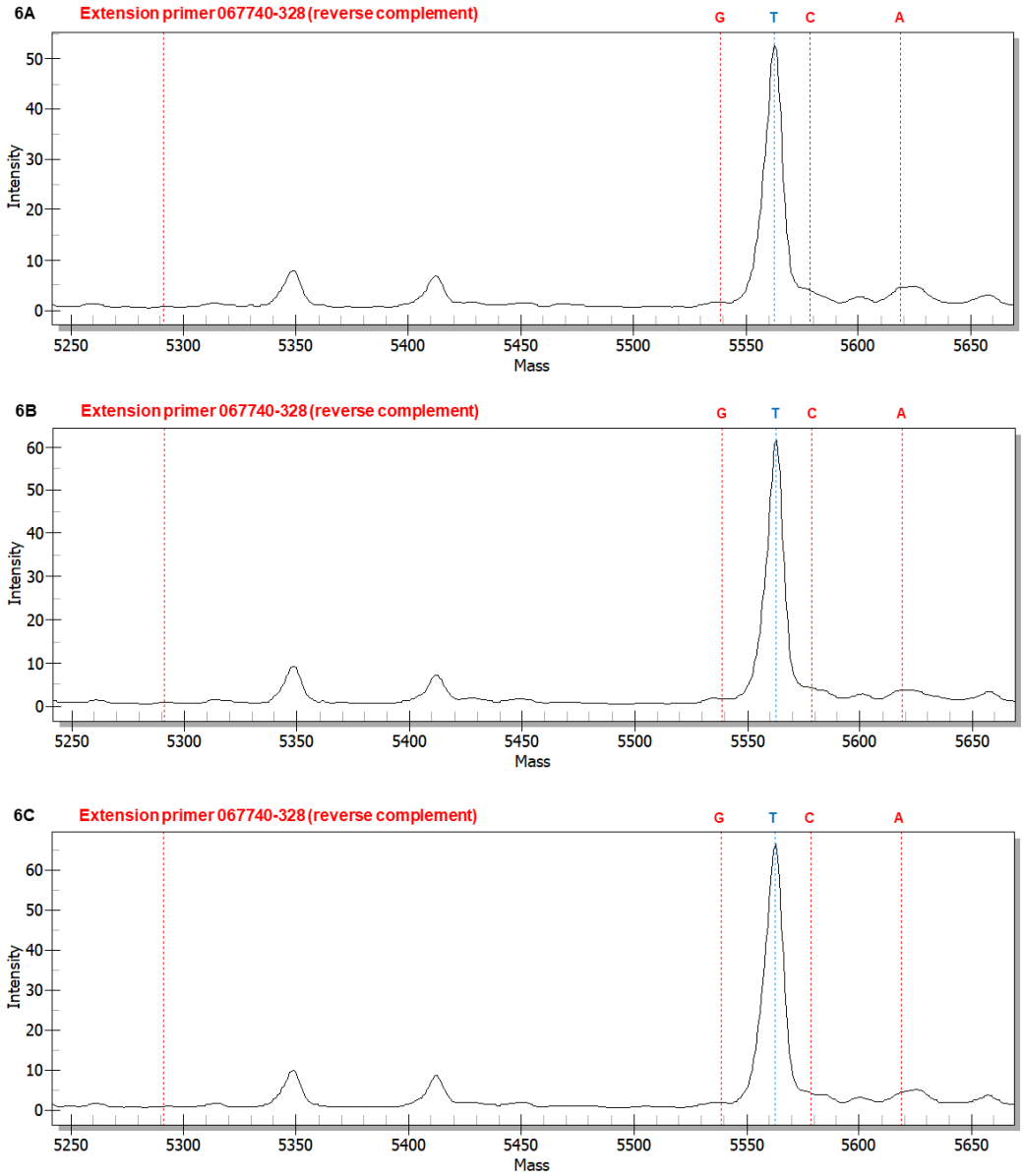

Fig 6. MALDI-TOF mass spectra of extension primer 067740-328 (reverse complement) to distinguish between the AT-genotypes in the SFPs (with ascocarps) prior to and after ascospore ejection and of developmental failure. The extension reaction proceeded from extension primer 067740-328 (reverse complement) toward the SNP at position 328 in the AB067740 sequence (*cf.* Fig 1 for the location). In the allelic peaks, "G" represents the primer with an extended reverse complement cytosine (guanine in the sense chain; *cf.* Fig 1); "T" represents an extended reverse complement adenine (thymine in the sense chain); "C" denotes an extended reverse complement guanine (cytosine in the sense chain); and "A" indicates an extended reverse complement thymine (adenine in the sense chain). Panel 6A shows the mass spectrum of the pre-ejection SFP. Panel 6B shows the mass spectrum of the post-ejection SFP. Panel 6C shows the mass spectrum of the SFP of developmental failure.

Table 5. Mass intensity ratios of the SNP allelic peaks of transition and transversion mutant genotypes in SFPs prior to and after ascospore ejection and of developmental failure

Extension primer	Allelic ratio	Intensity ratio		
		Prior-ejection SFP (*cf.* Fig 6A)	**Post-ejection SFP** (*cf.* Fig 6B)	**SFP of developmental failure** (*cf.* Fig 6C)
067740-328	T:C	14.1 (52.0÷3.7)	16.5 (↔; 61.0÷3.7)	19.3 (↑; 65.5÷3.4)
	T:G	—	—	—
	T:A	11.1 (52.0÷4.7)	20.3 (↑; 61.0÷3.0)	17.7 (↑; 65.5÷3.7)

Note: In the primer 067744-328 section (upper panel), Peak T represents AT-biased Genotypes #5 and #15 of *O. sinensis,* and Peak C indicates AT-biased Genotype #4 of *O. sinensis* (*cf.* Fig 1). In the primer 067744-324 section (lower panel), Peak C represents AT-biased Genotype #5 of *O. sinensis,* and Peak T indicates other AT-biased genotypes of *O. sinensis*. Peaks G and A in both panels denote 2 transversion mutation genotypes of unknown sequences. "↔" indicates no significant change (within 20% variation), and "↑" denotes increases not greater than 2 times in intensity ratios compared to that for the pre-ejection SFP. "—" means that one of the allelic peaks was missing, and no ratio could be calculated.

Using extension primer 067744-324 to distinguish between AT-biased Genotypes #5 and #15

Peak C with extremely low intensities in Figs 6A–6C for all 3 SFP samples indicated a consistently low quantity of Genotype #4 of AT-biased Cluster-B, consistent with the report by Li et al. [61] based on the use of genotype-specific primers and cloning-based PCR amplicon sequencing techniques. A stratified genotyping strategy was then applied using extension primer 067744-324 (*cf.* Table 2) to further analyze the extremely high-intensity Peak T shown in Fig 6, representing Genotypes #5–6 and #15.

Fig 7A shows a mass spectrum of extension primer 067744-324 (reverse complement) (*cf.* Table 2) for the pre-ejection SFP. Peak T possessing extremely high intensity represented Genotypes #6 and #15 (*cf.* Fig 1), while the component Genotype #4 was attributed only to a very small portion of Peak T, as demonstrated in Fig 6 and Table 5. Although the extension reaction of primer 067744-324 could also result in an extended cytosine on the DNA templates of Genotype #16 (*cf.* Fig 1), this genotype was absent in the SFPs of natural *C. sinensis* when using genotype-specific primers and PCR amplicon-cloning techniques [61]. Peak C possessing the second highest intensity represented Genotypes #5, although an extended cytosine may be produced in the extension reaction on the DNA templates of Genotype #17 using primer 067744-324, this genotype was absent in the *C. sinensis* SFP when using genotype-specific primers and PCR amplicon-cloning techniques [61] (*cf.* Fig 1). Peaks C and T presented a C:T intensity ratio of 0.71 (Table 6). Peak G was absent. Peak A showed a low intensity, resulting in a C:A intensity

481 ratio of 4.56 (Table 6), representing a co-occurring transversion point mutation genotype of an unknown
482 sequence.

483 Fig 7B shows a mass spectrum for the post-ejection SFP, displaying a high intensity of Peak C
484 (Genotype #5). Peak T, representing Genotypes #6 and #15, appeared in the mass spectrum as a shoulder
485 of the acceding loop and was dramatically attenuated relative to that shown in Fig 7A, resulting in a
486 significantly elevated C:T ratio of 10.6 (Table 6). Peak G showed a low intensity, resulting in a C:G ratio
487 of 53, while Peak A remained at a low level with an elevated C:A ratio of 7.57 (Table 6).

488 Fig 7C shows a mass spectrum for the SFP of developmental failure. The mass spectrum topology
489 was similar to that shown in Fig 7B, except that the intensity of Peak C (Genotype #5) was further elevated,
490 resulting in a further elevated C:T ratio (Table 6). Peak G was nearly flat and negligible, while Peak A
491 remained at a low intensity, with an elevated C:A ratio of 8.50 (Table 6).

492 Fig 7D shows the overlapping mass spectra of Figs 7A and 7B after adjusting and aligning the vertical
493 axis for intensity and visualizes the dynamic alteration of the allelic peaks in the SFPs from pre-ejection
494 to post-ejection.

495 In contrast to the consistently low levels of Genotype #4 in all 3 SFP samples shown in Fig 6, the
496 stratified analysis indicated dramatic alterations of Peak T, which showed a very high level in the pre-
497 ejection SFP but presented significant attenuation in the SFPs after ejection and of developmental failure
498 (Fig 7). Peak T represents the sum of intensities of Genotypes #6 and #15. Both Genotypes #4 and #15 of
499 AT-biased Cluster-B were present in the *C. sinensis* SFP but absent in ascospore samples, as demonstrated
500 by Li et al. [59,61]. In contrast, Genotype #5 of AT-biased Cluster-A, which was represented by Peak C in
501 Fig 7, showed a consistently high intensity in all SFP samples. Transversion mutation genotypes of
502 unknown sequences either remained at a constantly low level (Peak A) or were absent (Peak G) in the SFP
503 samples. Genotype #6 of AT-biased Cluster-A underwent dynamic quantitative alteration along with
504 Genotype #15 of AT-biased Cluster-B when comparing Peak T in Figs 7A and 7B. Genotype #6 was
505 clustered phylogenetically in the clade of AT-biased Cluster-A as shown in Fig 2, but it is closer to the
506 clade of AT-biased Cluster-B compared with other genotypes in AT-biased Cluster-A, indicating a certain
507 symbiosis of Genotype #6 in the sexual life of *O. sinensis* somewhat similar to AT-biased Cluster-B
508 genotypes.

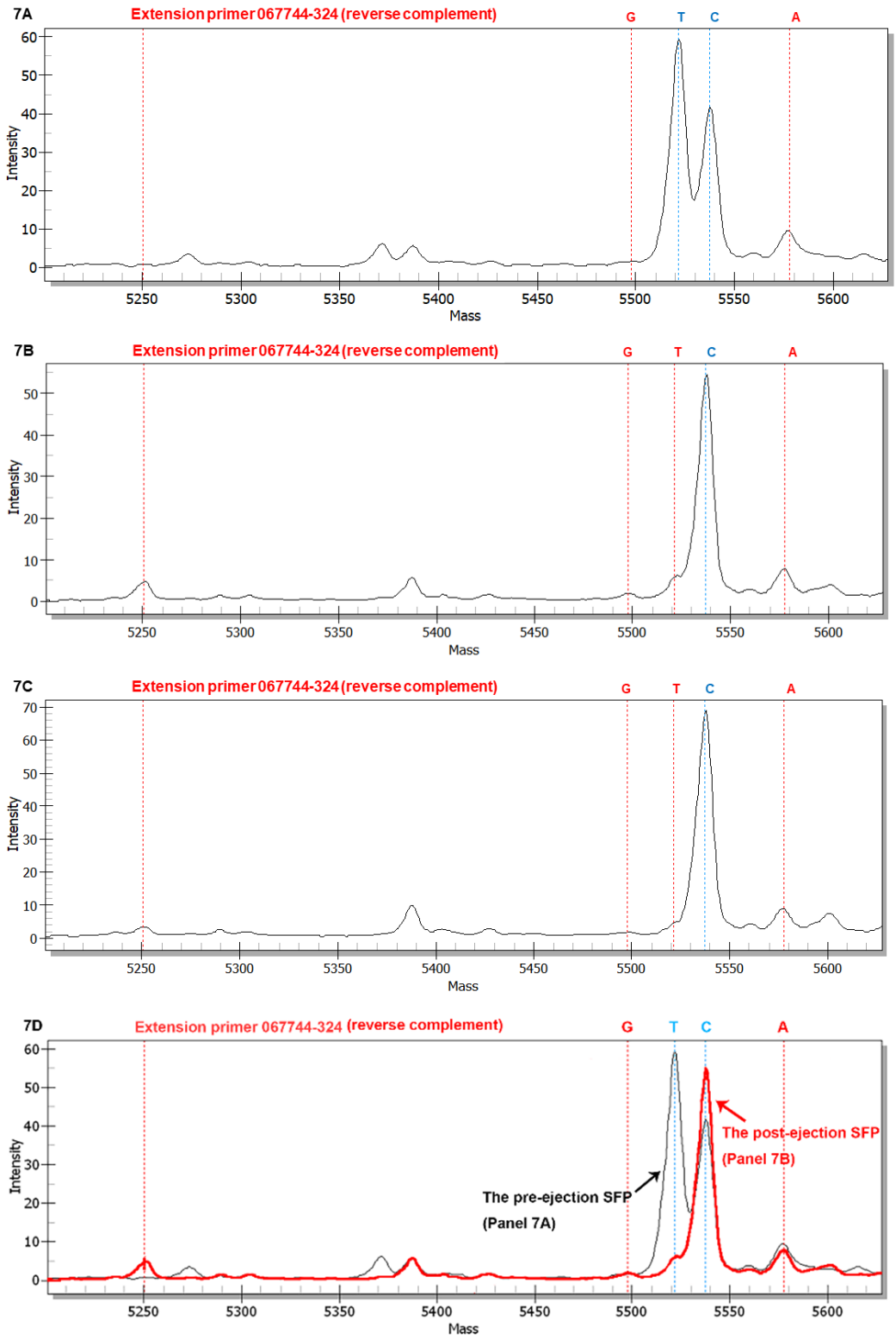

Fig 7. MALDI-TOF mass spectra of extension primer 067744-324 (reverse complement) to distinguish between the AT-biased genotypes in the SFPs (with ascocarps) prior to and after ascospore ejection and of developmental failure. The extension reaction proceeded from extension primer 067744-324 (reverse

complement) toward the SNP at position 324 in the AB067740 sequence (*cf.* Fig 1 for the location). In the allelic peaks, "G" represents the primer with an extended reverse complement cytosine (guanine in the sense chain; *cf.* Fig 1); "T" represents an extended reverse complement adenine (thymine in the sense chain); "C" denotes an extended reverse complement guanine (cytosine in sense chain); and "A" indicates an extended reverse complement thymine (adenine in the sense chain). Panel 7A shows the mass spectrum of the pre-ejection SFP. Panel 7B shows the mass spectrum of the post-ejection SFP. Panel 7C shows the mass spectrum of the SFP of developmental failure. Panel 7D shows the overlapping mass spectra for Panels 7A (black tracing) and 7B (red tracing) with alignment of the horizontal and vertical axes of the panels.

Table 6. Mass intensity ratios of the SNP allelic peaks of transition and transversion mutant genotypes in SFPs prior to and after ascospore ejection and of developmental failure

Extension primer	Allelic ratio	Intensity ratio		
		Prior-ejection SFP (*cf.* Fig 7A)	**Post-ejection SFP** (*cf.* Fig 7B)	**SFP of developmental failure** (*cf.* Fig 7C)
067744-324	C:T	0.71 (41÷58)	10.6 (↑↑↑↑; 53÷5.0)	15.1 (↑↑↑↑; 68÷4.5)
	C:G	—	53.0 (53÷1.0)	—
	C:A	4.56 (41÷9.0)	7.57 (↑; 53÷7.0)	8.50 (↑; 68÷8.0)

Note: In the primer 067744-328 section (upper panel), Peak T represents AT-biased Genotypes #5 and #15 of *O. sinensis,* and Peak C indicates AT-biased Genotype #4 of *O. sinensis* (*cf.* Fig 1). In the primer 067744-324 section (lower panel), Peak C represents AT-biased Genotype #5 of *O. sinensis,* and Peak T indicates other AT-biased genotypes of *O. sinensis*. Peaks G and A in both panels denote 2 transversion mutation genotypes of unknown sequences. "↑" (increase not greater than 2 times) and "↑↑↑↑" (increase greater than 4 times) denote significant increases in intensity ratios compared to that for the pre-ejection SFP. "—" means that one of the allelic peaks was missing, and no ratio could be calculated.

SNP genotyping analysis to distinguish between the GC- and AT-biased genotypes of *O. sinensis* in the fully and semi-ejected ascospores

Li et al. [61] reported the detection of Genotype #13 in semi-ejected ascospores but not in fully ejected ascospores and the detection of Genotype #14 in fully ejected ascospores but not in semi-ejected ascospores. These 2 offspring genotypes of *O. sinensis* were characterized by large DNA segment reciprocal substitutions and genetic material recombination between 2 parental fungi (Group A *H. sinensis* and an AB067719-type Group E fungus [8–10,61]). The ITS1-5.8S-ITS2 sequences of Genotypes #13–14 were alternatively segmentally inherited from their parental fungi [61]. The segment sequences of Genotypes #13–14 are either completely identical to or far different from those of Genotype #1, and the primer pairs for the first-step PCR listed in Table 1 are unfavorable for amplifying the ITS sequences of Genotypes #13–14. Thus, the genotyping study presented herein does not cover the analysis of GC-biased Genotypes #13–14.

Fig 8A shows a mass spectrum of extension primer 067721-477 (*cf.* Table 2) for fully ejected ascospores. Peak G represents GC-biased Genotype #1 (*cf.* Fig 1). Peak A represents transition point mutation AT-biased genotypes. Peak C was absent. Peak T had a very low intensity, representing a transversion point mutation genotype of an unknown sequence. The primers employed for the first-step PCR preferentially amplified the sequences of GC-biased genotypes, producing an amplicon pool containing sequences of GC-biased genotypes in greater quantities than the AT-biased sequences. The amplicon pool was used as the template for the second-step PCR, showing the higher-intensity Peak G and the lower-intensity Peak A. The G:A and G:T ratios were 2.5 and 15.0, respectively (Table 7).

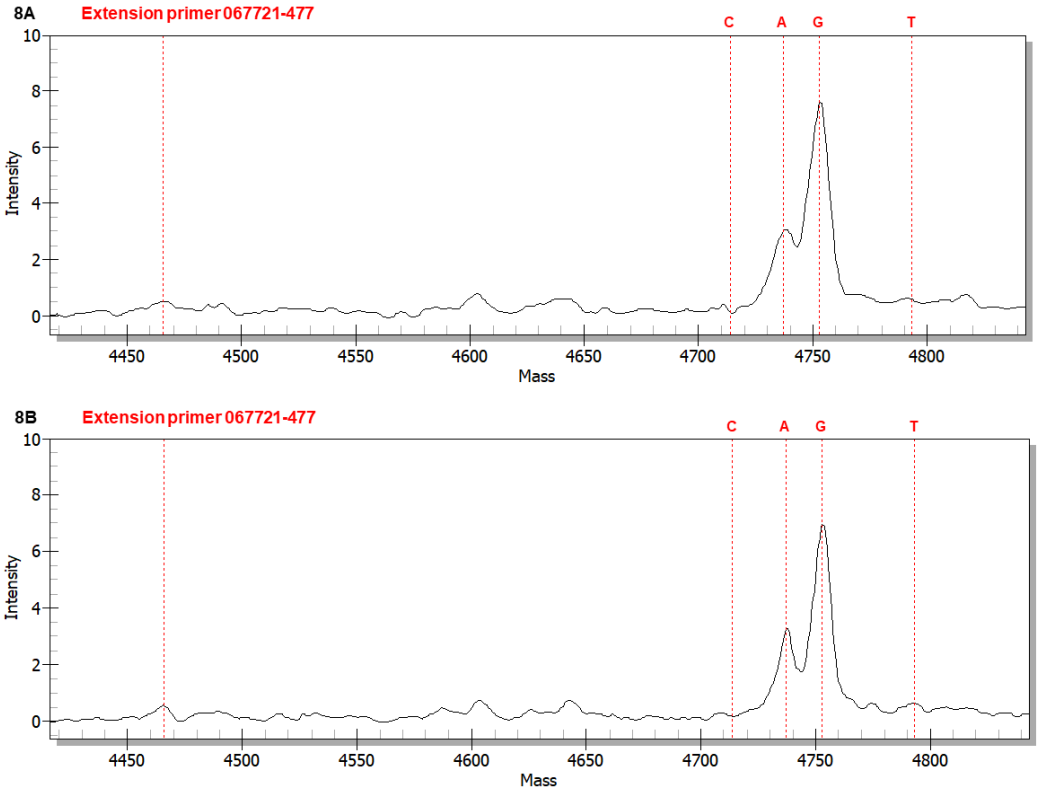

Fig 8. MALDI-TOF mass spectra of extension primer 067721-477 to distinguish between GC- and AT-genotypes in fully and semi-ejected ascospores. The extension reaction proceeded from extension primer 067721-477 toward the SNP at position 477 in the AB067721 sequence (*cf.* Fig 1 for the location). In the allelic peaks, "C" denotes the primer with an extended cytosine; "A" indicates an extended adenine; "G" represents an extended guanine; and "T" represents an extended thymine. Panel 8A shows the mass spectrum of fully ejected ascospores. Panel 8B shows the mass spectrum of semi-ejected ascospores.

Fig 8B shows a mass spectrum for the semi-ejected ascospores with a similar mass spec topology to that shown in Fig 8A. Peak G represents GC-biased Genotype #1, and Peak A represents AT-biased genotypes. There were no significant changes in the intensity ratios of G:A (2.2) and G:T (13.8) relative to those for the fully ejected ascospores (Table 7). Peak C was absent.

562 **Table 7. Mass intensity ratios of the SNP allelic peaks of transition and transversion mutant genotypes in**
563 **fully and semi-ejected ascospores**

Extension primer	Allelic ratio	Intensity ratio	
		Fully ejected ascospores	**Semi-ejected ascospores**
067721-477		(*cf.* Fig 8A)	(*cf.* Fig 8B)
	G:A	**2.5** (7.5÷3.0)	**2.2** (↔; 6.7÷3.2)
	G:C	—	—
	G:T	**15.0** (7.5÷0.5)	**13.8** (↔; 6.9÷0.5)

564 Note: Peak G represents GC-biased Genotype #1 *H. sinensis*; Peak A indicates AT-biased genotypes of *O. sinensis*
565 (*cf.* Fig 1). Peaks C and T denote 2 transversion mutation genotypes of unknown sequences. "↔" indicates no
566 significant change (within 20% variation) compared to the intensity ratios for fully ejected ascospores. "—" means that
567 one of the allelic peaks was missing, and no ratio could be calculated.

568 The extension primer 067721-531 (*cf.* Table 2) was also used to distinguish between the GC- and AT-
569 biased genotypes of *O. sinensis* in the fully and semi-ejected ascospores. Mass spectra (not shown) showed
570 the same topologies of Peaks A and G as shown in both panels of Fig 8, except for the absence of both
571 Peaks C and T representing transversion alleles. There was no meaningful change in the G:A intensity
572 ratio (Table 8).

573 **Table 8. Mass intensity ratios of the SNP allelic peaks of transition and transversion mutant genotypes in**
574 **fully and semi-ejected ascospores**

Extension primer	Allelic ratio	Intensity ratio	
		Fully ejected ascospores (Mass spectrum not shown)	**Semi-ejected ascospores** (Mass spectrum not shown)
067721-531	G:A	**18.3** (5.5÷0.3)	**16.0** (↔; 8.0÷0.5)
	G:C	—	—
	G:T	—	—

575 Note: Peak G represents GC-biased Genotype #1 *H. sinensis*; Peak A indicates AT-biased genotypes of *O. sinensis*
576 (*cf.* Fig 1). Peaks C and T denote 2 transversion mutation genotypes of unknown sequences. "↔" indicates no
577 significant change (within 20% variation) compared to the intensity ratios for fully ejected ascospores. "—" means that
578 one of the allelic peaks was missing, and no ratio could be calculated.

579

580 SNP genotyping analysis to distinguish between the AT-biased genotypes of
581 *O. sinensis* in fully and semi-ejected ascospores

582 Li et al. [61] reported the absence of genotypes of AT-biased Cluster-B (Genotypes #4 and #15; *cf.*
583 Fig 2) in the 2 types of ascospores. SNP genotyping using extension primer 067740-328 (reverse

complement) (*cf*. Table 2) confirmed that both mass spectra (not shown) for the fully and semi-ejected ascospores showed a single Peak T of high intensity, representing Genotypes #5–6 and #16 of AT-biased Cluster-A (*cf*. Fig 2) [61]. Peaks C (Genotype #4 of AT-biased Cluster-B) and G (a transversion allele of an unknown sequence) are nearly flat. Peak A with very low intensities indicated the co-occurrence of a transversion mutation genotype of an unknown sequence in both ascosporic samples. The increase in the T:A ratio from 14.0 in fully ejected ascospores to 22.0 (Table 9) in semi-ejected ascospores was due to the considerably increased intensity of Peak T, the genotypes of AT-biased Cluster-A.

Table 9. Mass intensity ratios for the SNP allelic peaks for multiple transition and transversion mutation genotypes in the fully and semi-ejected ascospores

Extension primer	Allelic ratio	Intensity ratio	
		Fully ejected ascospores (Mass spectrum not shown)	Semi-ejected ascospores (Mass spectra not shown)
067740-328	T:C	—	—
	T:A	**14.0** (42.0÷3.0)	**22.0** (↑; 66÷3.0)
	T:G	—	—

Note: In the 067740-328 primer section (upper panel), Peak T represents AT-biased Genotype #4 of *O. sinensis,* and Peak T indicates other AT-biased genotypes of *O. sinensis* (*cf*. Fig 1). In the 067740-324 primer section (lower panel), Peak C represents AT-biased Genotype #5 of *O. sinensis,* and Peak T indicates other AT-biased genotypes of *O. sinensis* (*cf*. Fig 1). Peaks G and A in both panels denote 2 transversion mutation genotypes of unknown sequences. "↑" indicates a significant increase not greater than 2 times in the intensity ratio compared to that of the fully ejected ascospores. "—" means missing one of the allele peaks, and no ratio could be calculated.

Fig 9A shows a mass spectrum obtained using extension primer 067740-324 (*cf*. Table 2) from the fully ejected ascospores. Peak C represented AT-biased Genotype #5 (*cf*. Fig 1), while AT-biased Genotype #17, with the same extended cytosine, was absent in the ascospores based on the use of genotype-specific primers and cloning-based amplicon sequencing [61]. Peak T represented AT-biased Genotypes #6 and #16 of AT-biased Cluster-A, while Genotypes #4 and #15 of AT-biased Cluster-B, with the same extended thymine, were absent in the ascospores [61]. The lower intensity of Peak C and the higher intensity of Peak T resulted in a C:T ratio of 0.69 (Table 10). Peaks A and G represent low-intensity transversion point mutation genotypes of unknown sequences, with C:A and C:G ratios of 9.06 and 15.4, respectively (Table 10).

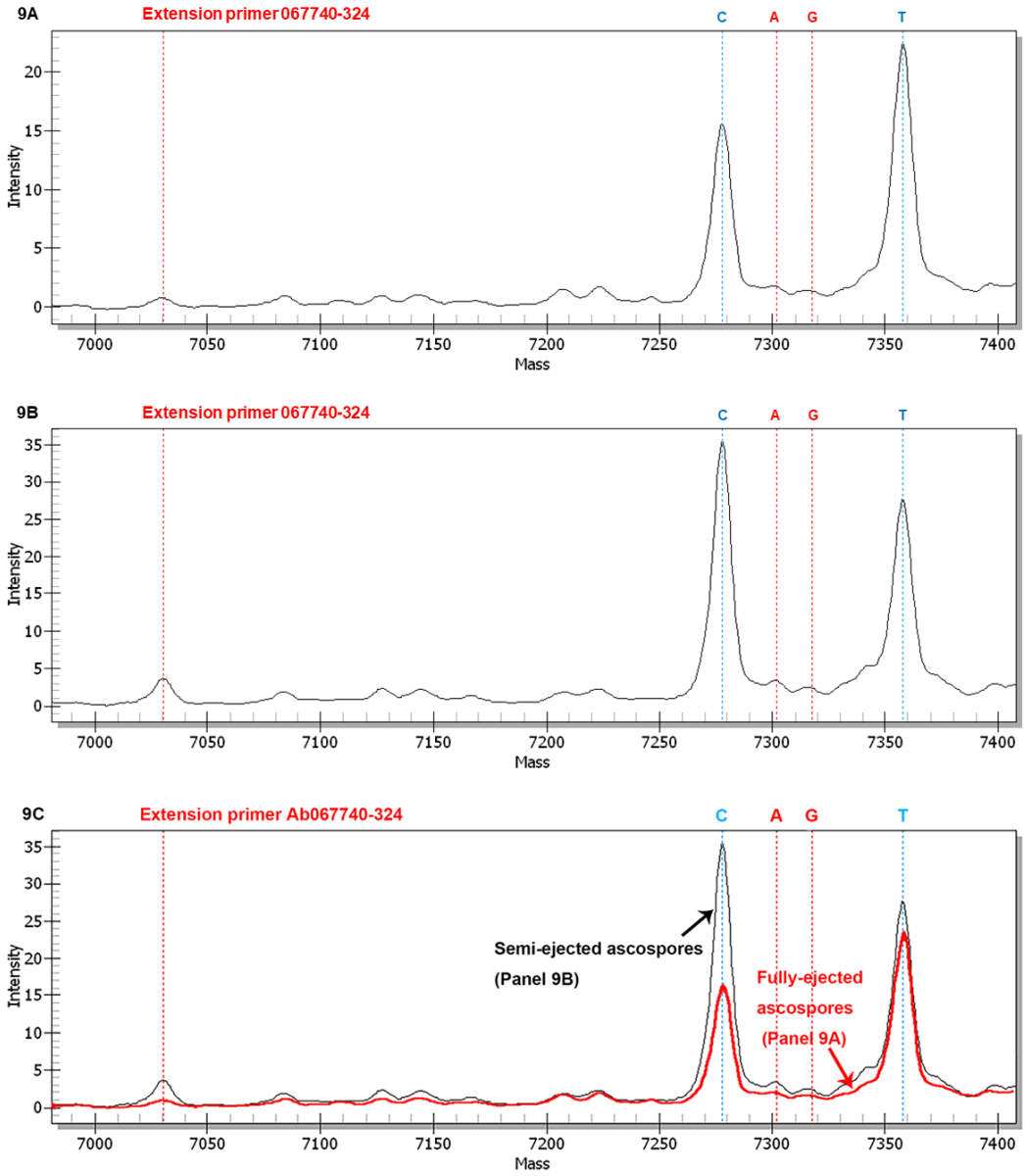

611

612 **Fig 9. MALDI-TOF mass spectra of extension primer 067740-324 to distinguish between AT-biased**
613 **genotypes in the fully and semi-ejected ascospores.** The extension reaction proceeded from extension primer
614 067740-324 toward the SNP at position 324 in the AB067740 sequence (*cf.* Fig 1 for the location). In the allelic
615 peaks, "C" denotes the primer with an extended cytosine; "A" indicates an extended adenine; "G" represents an
616 extended guanine; and "T" indicates an extended thymine. Panel 9A shows the mass spectrum of fully ejected
617 ascospores. Panel 9B shows the mass spectrum of semi-ejected ascospores. Panel 9C shows the overlapping mass
618 spectra for Panels 9A (black tracing) and 9B (red tracing) with alignment of the horizontal and vertical axes of the
619 panels.

620 Fig 9B shows a mass spectrum for semi-ejected ascospores. The intensity of Peak C (Genotype #5)
621 was elevated more than doubled, from 15.4 in fully ejected ascospores to 34.8 in semi-ejected ascospores,
622 as visualized in Fig 9C after adjusting and aligning the vertical axis for intensity for the overlapping mass
623 spectra of Figs 9A and 9B. Peak T (Genotypes #6 and #16) was slightly elevated from 22.3 to 26.8 (Figs

9A–9C). The asynchronous, disproportional increases in intensity resulted in a dynamic elevation of the C:T ratio from 0.69 to 1.30 from the fully ejected ascospores to the semi-ejected ascospores (Table 10). The intensities of Peaks A and G were slightly increased, resulting in increases in the C:A and C:G intensity ratios from 9.06 to 14.5 and 15.4 to 18.3, respectively (Table 10), due to the considerably elevated intensity of Peak C.

Table 10. Mass intensity ratios for the SNP allelic peaks for multiple transition and transversion mutation genotypes in the fully and semi-ejected ascospores

Extension primer	Allelic ratio	Intensity ratio	
		Fully ejected ascospores (*cf.* Fig 9A)	**Semi-ejected ascospores** (*cf.* Fig 9B)
067740-324	C:T	**0.69** (15.4÷22.3)	**1.30** (↑; 34.8÷26.8)
	C:A	**9.06** (15.4÷1.7)	**14.5** (↑; 34.8÷2.4)
	C:G	**15.4** (15.4÷1.0)	**18.3** (↑; 34.8÷1.9)

Note: In the 067740-328 primer section (upper panel), Peak T represents AT-biased Genotype #4 of *O. sinensis,* and Peak T indicates other AT-biased genotypes of *O. sinensis* (*cf.* Fig 1). In the 067740-324 primer section (lower panel), Peak C represents AT-biased Genotype #5 of *O. sinensis,* and Peak T indicates other AT-biased genotypes of *O. sinensis* (*cf.* Fig 1). Peaks G and A in both panels denote 2 transversion mutation genotypes of unknown sequences. "↑" indicates a significant increase not greater than 2 times in the intensity ratio compared to that of the fully ejected ascospores. "—" means missing one of the allele peaks, and no ratio could be calculated.

Discussion

Natural *C. sinensis* is an integrated microecosystem of the insect-fungal complex, and its metagenomic members are differentially alternated in different combinations and play different biological roles in its complicated lifecycle [19]. Along with multiple fungal species, 17 genotypes of *O. sinensis* of genetically and phylogenetically distinct (*cf.* Figs 1–2) have been identified, which differentially co-occur in the stroma, caterpillar body, SFP (with ascocarps) and ascospores of natural *C. sinensis* [6–10,12–16,19–21,27–32,37,48–50,57–59,61]. This study has examined teleomorphic genotypes of *O. sinensis*, which differentially occur and are dynamically altered in the SFPs and ascospores of natural *C. sinensis*, the sexual organ and reproductive cells.

Biochip-based MassARRAY mass spectrometry SNP genotyping technique

651 The stroma and caterpillar body of *C. sinensis* have been examined using the Southern blotting
652 technique, and the natural abundance without DNA amplification of GC- and AT-biased genotypes of *O.*
653 *sinensis* have been found to exhibit dynamic alterations in an asynchronized and disproportional manner
654 in the compartments of *C. sinensis* during maturation [6–10,15–16,22]. Southern blotting analysis is not
655 believed to be supersensitive but is able to demonstrate the natural abundance of DNA species in test
656 materials, directly reflecting the natural biomasses of the target DNA moieties. Although PCR-based
657 techniques are considered sensitive molecular approaches, they may lead to disproportional exponential
658 amplifications and inaccurate quantifications of various metagenomic components in complex DNA
659 samples because of the involvement of multiple technical factors influencing the PCR process and
660 sometimes cause failure of DNA amplification and sequencing for various reasons [6–10,15–16,22].

661 We designed two types of PCR-based experiments in this research project: (1) qualitative
662 examinations using multiple sets of species- and genotype-specific primers for touch-down PCR and
663 cloning-based amplicon sequencing to profile the genotypic components of the metagenomic DNA
664 extracted from different compartments of natural *C. sinensis* in different development and maturation
665 stages, as presented in the companion paper [61]; and (2) a semiquantitative analysis using SNP mass
666 spectrometry genotyping to semiquantitatively monitor the dynamic alterations of the various genotypes,
667 as presented herein in this paper.

668 Secondary structures/conformation in ITS1-5.8S-ITS2 sequences of *O. sinensis* genotypes have been
669 recognized previously and greatly impact and even perplex PCR amplification and amplicon sequencing,
670 often causing false negative results and consequently incorrect conclusions [7–10,15,19–20,59].
671 MassARRAY SNP MALDI-TOF MS genotyping represents a useful technique to overcome the
672 shortcomings of regular PCR identification. It is a two-step PCR-mass spectrometry technique involving
673 a 384-well biochip [15,19–20,68,72]. Sequences containing various SNP alleles of different genotypes
674 may not be amplified at the same rate because of (1) different amounts of DNA templates (*i.e.*, the
675 amplicons obtained from the first-step PCR) in the samples, (2) variable DNA sequences and related
676 secondary structures, (3) different primer binding rates and DNA chain extension rates, causing the MS
677 intensities of the SNP alleles to not directly reflect the copy numbers of the genotypic sequences, and (4)
678 perhaps other reasons in the natural world. However, under the same PCR conditions using the same pair
679 of first-step primers, the same second-step extension primer, and the same batch of reaction buffer run
680 according to the same PCR settings and extension reaction on a single 384-well chip, the sequences of
681 each genotype will be amplified at comparable rates from one reaction well to another in a single chip.

682 Although direct quantitative comparisons of the intensities of the same allelic peaks in different mass
683 spectra may not be accurate, it is possible to select the intensity of one SNP allelic peak in each of the
684 mass spectra as the internal reference for computing intensity ratios (Tables 3–x10), which provides
685 legitimate information for semiquantitative comparisons of the relative abundances of genotypes in
686 different mass spectra and semiquantitative monitoring of the alterations of the genotypes among the study
687 samples. Such semiquantitative comparisons of intensity ratios are logical and valid within a systematic
688 error, reflecting the relative alterations of GC- and AT-biased genotypes of *O. sinensis* and the transversion
689 mutation genotypes of unknown sequences in the SFPs prior to and after ascospore ejection and of
690 developmental failure and in fully and semi-ejected ascospores collected from the same *C. sinensis*
691 specimens.

692

693 **Dynamic alterations of the genotypes of *O. sinensis***

694 Southern blotting, restriction fragment length polymorphism (RFLP) analysis combined with
695 amplicon sequencing, SNP genotyping, and other molecular examinations demonstrated that GC-biased
696 Genotype #1 *H. sinensis* was never the dominant fungal species in the *C. sinensis* stroma and that AT-
697 biased genotypes were the dominant species [6–10,15–16,19–21,61,67]. Li et al. [59] proposed that all
698 AT-biased genotypes are "ITS pseudogenes … in a genome" of Genotype #1 *H. sinensis*. However, the
699 sequences of Genotypes #2–17 do not reside in the genome assemblies (ANOV00000000, NGJJ00000000,
700 LKHE00000000, LWBQ00000000, and JAAVMX000000000) of *H. sinensis* Strains Co18, CC1406-203,
701 1229, ZJB12195, and IOZ07, respectively, but instead belong to the genomes of independent *O. sinensis*
702 fungi [6–10,13,15–16,19–21,47–54,61,67]. The dynamic alterations of GC- and AT-biased genotypes of
703 *O. sinensis* in the asynchronous, disproportional manner observed in this study (*cf*. Figs 4–9) and previous
704 studies further confirmed the genomic independence of the multiple genotypes, providing evidence of the
705 existence of independent *O. sinensis* fungi, which thus disproved the "ITS pseudogenes … in a single
706 genome" hypothesis that was based on the misinterpretation of genomic residency data for the multiple
707 AT-biased mutant genotypes in the genome of GC-biased Genotype #1 *H. sinensis* [6–10,13,15–16,47–
708 54,61].

709 This study further revealed the differential co-occurrence and dynamic alterations of GC- and AT-
710 biased genotypes in the SFPs (with ascocarps) and ascospores of natural *C. sinensis* (*cf*. Figs 4–9). For

711 instance, Fig 5A demonstrates the nearly identical intensities of Peaks A and G, representing GC- and AT-
712 biased genotypes of *O. sinensis*, in the pre-ejection SFP, and Fig 5B shows a significant reduction of Peak
713 A (AT-biased genotypes) after ascospore ejection (*cf.* Fig 5D), resulting in a dramatic increase in the G:A
714 intensity ratio (*cf.* Table 4). Figs 9A–9C demonstrate that Peak C (AT-biased Genotype #5) with slightly
715 lower intensity in the fully ejected ascospores increased more than doubled in the semi-ejected ascospores
716 collected from the same pieces of natural *C. sinensis*, while Peak T (AT-biased Genotypes #6 and #16)
717 with higher intensity in the fully ejected ascospores increased slightly in the semi-ejected ascospores (*cf.*
718 Table 10). Genotypes #5–6 and #16 were phylogenetically clustered into AT-biased Cluster-A (*cf.* Fig 2).
719 Significant changes in the intensities of AT-biased genotypes are also shown in other figures and tables,
720 indicating that the sequences of AT-biased genotypes belong to the genomes of independent *O. sinensis*
721 fungi.

722 The dynamic alterations of the intensities of the allelic peaks suggested the genomic independence of
723 GC- and AT-biased *O. sinensis* genotypes, inconsistent with the hypothesis that multiple AT-biased "ITS
724 pseudogene" components of *O. sinensis* belong to "a single genome" of Genotype #1 *H. sinensis* [48,50].
725 Notably, the intensities of the allelic peaks and their alterations shown in Figs 4–5 and 8 do not necessarily
726 reflect the natural biomasses of the GC- and AT-biased genotypes of *O. sinensis* because the primers
727 employed for the first-step PCR preferentially amplified GC-biased genotypes over AT-biased genotypes,
728 producing a greater amount of GC-biased amplicons that served as the templates for primer extension
729 reactions in the second-step PCR.

730 Mass spectra obtained using extension primers 067721-447 and 067721-531 demonstrated the co-
731 occurrence of GC- and AT-biased *O. sinensis* genotypes in fully and semi-ejected ascospores, resulting in
732 essentially unchanged G:A ratios (*cf.* Fig 8, Tables x7–x8).

733 GC-biased Genotype #1 *H. sinensis* is postulated to be an anamorph of *O. sinensis* [39], although it
734 may not be the sole anamorph [6–10,48,50,67]. In addition, GC-biased Genotype #1 was reported to be
735 the sole teleomorph of *O. sinensis* in natural *C. sinensis* [39,46], and AT-biased Genotype #4 was the sole
736 teleomorph of *O. sinensis* in cultivated *C. sinensis* [46]. Our findings presented in this paper indicate that
737 multiple co-occurring teleomorphic AT-biased genotypes may play critical symbiotic roles in the
738 development and maturation of SFPs with ascocarps and ascospores in the sexual life stage of *C. sinensis*.
739 Without certain AT-biased *O. sinensis* genotypes in various combinations, ascocarps may not be able to
740 normally develop and mature to support the development, maturation and ejection of the *C. sinensis*

741 ascospores (*cf*. Figs 4–7), especially lacking high intensities of Genotype #6 (AT-biased Cluster-A) and
742 Genotype #15 (AT-biased Cluster-B) in the SFPs of developmental failure, as shown in Fig 7C. We also
743 noticed the coexistence of transversion mutated alleles of unknown sequences that were altered in the
744 SFPs and ascospores (Figs 4–9; Tables 3–x10), suggesting that these genotypes may also participate
745 symbiotically in the development and maturation of ascocarps and ascospores.

746

747 **Stratification strategy for genotyping AT-biased genotypes**

748 The stratification genotyping strategy used in this study profiled multiple genotypic components of
749 AT-biased Clusters A and B in the *C. sinensis* SFPs. The first step of stratifying assays used extension
750 primer 067740-328. The mass spectra of the SFPs prior to and after ascospore ejection and of
751 developmental failure demonstrated the existence of an extremely small quantity of Genotype #4 of AT-
752 biased Cluster-B represented by Peak C in Figs 6A–6C, in addition to large amounts of Genotypes #5–6
753 of AT-biased Cluster-A and Genotype #15 of AT-biased Cluster-B. In contrast to the dominance of
754 Genotype #4 of AT-biased Cluster-B in the stroma of immature *C. sinensis*, in its asexual growth stage,
755 the abundance of Genotype #4 dramatically declined in the stroma of mature *C. sinensis* and retained its
756 very low level in the SFPs (with ascocarps) in the sexual stage of the *C. sinensis* lifecycle [15–16,19–
757 21,61].

758 The second step of the stratification analysis involved the extension primer 067744-324. Mass spectra
759 demonstrated a higher intensity of Peak T (sum of a minimal quantity of Genotype #4 and a high amount
760 of Genotypes #6 and #15) and a slightly lower intensity of Peak C (Genotype #5) in the pre-ejection SFP
761 (*cf*. Fig 7A), resulting in a C:T ratio of 0.7 (*cf*. Table 6). In contrast to retaining its high intensity of Peak
762 C (Genotype #5 of AT-biased Cluster-A) in the post-ejection SFP, Peak T was significantly attenuated
763 (*cf*. Figs 7B and 7D), representing a reduction in Genotype #6 (AT-biased Cluster-A) and Genotype #15
764 (AT-biased Cluster-B) along with the extremely small quantity of component Genotype #4 in the *C.*
765 *sinensis* SFP (*cf*. Fig 6); this caused a significant increase in the C:T ratio (*cf*. Table 6). Peak T (Genotypes
766 #4, #6 and #15) also showed extremely low intensity in the SFP of developmental failure, resulting in an
767 extremely high C:T ratio. These findings indicated that AT-biased Genotypes #6 and #15 may play critical
768 roles in the development and maturation of *C. sinensis* ascocarps and that insufficient Genotypes #6 and
769 #15 in the SFP may cause developmental failure of *C. sinensis* ascocarps (comparing Figs 7A and 7C)

770 compared to Genotype #4, which may play an important role in the early asexual developmental stage of
771 natural *C. sinensis* [61]. Genotypes #4 and #15 were phylogenetically clustered into AT-biased Cluster-
772 B. Genotype #6 was clustered into AT-biased Cluster-A but phylogenetically closer to Cluster-B than
773 other Cluster-A genotypes (*cf*. Fig 2).

774 Genotypes #4 and #15 of AT-biased Cluster-B were absent in the ascospores of *C. sinensis*, as
775 presented in a companion paper [61]. Genotype #5 (Peak C in Fig 9) and Genotypes #6 and #16
776 (components of Peak T) were phylogenetically clustered into AT-biased Cluster-A (*cf*. Fig 2) and play
777 symbiotic roles in assisting the function of GC-biased Genotype #1 *H. sinensis* in the sexual life stage of
778 natural *C. sinensis*, which is critical for the development, maturation and ejection of *C. sinensis*
779 ascospores.

780 This paper and its companion paper [61] demonstrated the symbiotic co-occurrence of GC-biased
781 Genotype #1 and AT-biased Genotypes #5–6 and #16 of *O. sinensis* in *C. sinensis* ascospores. However,
782 Li et al. [59] reported the detection of GC-biased Genotype #1 and AT-biased Genotype #5 in 8 of 15
783 clones in 25-day cultures generated from monoascospores. Apparently, the culture-dependent study by Li
784 et al. [59] overlooked AT-biased Genotypes #6 and #16 as well as GC-biased Genotype #14 in fully
785 ejected ascospores [61], which might be attributed to either nonculturability of these overlooked genotypes
786 of *O. sinensis* fungi under the 25-day *in vitro* culture conditions set by [59] or a failure of detection due to
787 an inappropriate design of the molecular methodology. As shown in Fig 1, the sequences of AT-biased
788 Genotypes #6 (EU555436) and #16 (KT232019) are both short compared with that of Genotype #1 *H.*
789 *sinensis*; Genotype #6 EU555436 is especially short, lacking short DNA segments close to its 5' and 3'
790 ends. There have been no reports of the detection of Genotypes #6 and #16 using universal primers. The
791 molecular features (secondary structure/conformation) of these genotypes may prevent their detection
792 when using universal primers [6–10,15–16,19–20].

793 Li et al. [61] reported the detection of Genotype #13 in semi-ejected ascospores and Genotype #14 in
794 fully ejected ascospores. These 2 GC-biased genetic variant genotypes feature large DNA segment
795 reciprocal substitutions and genetic material recombination between the 2 parental fungi (Group-A
796 Genotype #1 *H. sinensis* and an AB067719-type Group-E fungus), regardless of whether Genotypes #13–
797 14 are the offspring derived from fungal hybridization or parasexual reproduction [10,37]. Using
798 genotype-specific primers and cloning-based amplicon sequencing techniques is an appropriate approach
799 to identify the 2 offspring genotypes, as well as other AT-biased genotypes [61]. However, the

MassARRAY SNP mass spectrometry genotyping technique using the primer pairs and extension primers designed in this study is not applicable to identify ascosporic Genotypes #13–14 because the ITS1-5.8S-ITS2 sequences of Genotypes #13–14 were alternatively segmentally inherited from their parental fungi [61], either completely identical to or far different from those of Genotype #1 and the primer pairs for the first-step PCR (*cf*. Fig 1, Table 1). Thus, the semiquantitative study presented in this paper does not cover the analysis of GC-biased Genotypes #13–14.

True causative fungus/fungi of natural *C. sinensis*

Zhang et al. [71] summarized nearly 40 years of mycological experience involving the failed induction of the fruiting body and ascospore production in research-oriented laboratory settings, either in fungal cultures or after infecting insects with fungal inoculants. Hu et al. [47] reported success in inducing infection-mortality-mummification in 40 larvae of *Hepialus* sp. in an experiment using a mycelial mixture of anamorphic *H. sinensis* Strains Co18 and QH195-2 as inoculants but failed to induce the production of fruiting bodies.

Li et al. [72] demonstrated that a mixture of wild-type Strains CH1 and CH2 induced a favorable infection-mortality-mummification rate of 55.2±4.4% in 100 larvae of *Hepialus armoricanus*, which represents a 15–39-fold greater inoculation potency than the rates (1.4–3.5%) achieved after inoculation with the conidia or mycelia of *H. sinensis* or pure ascospores of *C. sinensis* (n=100 larvae in each inoculation experiment; $P<0.001$). The wild-type CH1 and CH2 strains exhibit *H. sinensis*-like morphological and growth characteristics but contain GC-biased Genotype #1 *H. sinensis*, AT-biased Genotype #4–6 of *O. sinensis*, and *Samsoniella hepiali* (synonym *Paecilomyces hepiali* [73]).

Wei et al. [46] reported an industrial artificial inoculation project and demonstrated a species contradiction between the anamorphic inoculant GC-biased Genotype #1 *H. sinensis* (Strains 130508-KD-2B, 20110514 and H01-20140924-03) and the sole teleomorph of AT-biased Genotype #4 of *O. sinensis* in cultivated *C. sinensis*. In addition to reporting the sole teleomorph of AT-biased Genotype #4 in cultivated *C. sinensis*, Wei et al. [46] also reported the sole teleomorph of GC-biased Genotype #1 in natural *C. sinensis*, reporting 2 teleomorphs of *O. sinensis*.

We reported the co-occurrence and dynamic alterations of multiple genotypes of *O. sinensis* in the teleomorphic SFPs and ascospores of natural *C. sinensis* in this study and the companion study [61],

829 suggesting that Genotype #1 is not the sole teleomorph of *O. sinensis* and that Genotype #1 *H. sinensis*
830 may be among the true causative fungi for natural and cultivated *C. sinensis*. Our findings of multiple
831 teleomorphs of *O. sinensis* may explain the 40-year failure of induction of the fruiting body and ascospore
832 production, as summarized by Zhang et al. [71]. The evidence from the studies [46–47,61,71–72]
833 suggested that the synergistic inoculation of multiple fungal species is required to initiate the development
834 of the stromal primordia and fruiting bodies of natural and cultivated *C. sinensis* and to subsequently
835 achieve the biological transition from the initial asexual growth to sexual reproduction in the later
836 maturational stages and complete the *O. sinensis* infection cycle and the natural *C. sinensis* lifecycle.

837

838 Inability of self-fertilization reproductive behavior in *H. sinensis*

839 The reproductive behavior of ascomycetes is controlled by transcription factors encoded at the
840 mating-type (*MAT*) locus [74–76]. The expression of mating genes is controlled at the genomic,
841 transcriptomic, proteomic, and posttranslational levels [37]. Zhang & Zhang [77] reported the differential
842 occurrence of mating-type genes of *MAT1-1* and *MAT1-2* idiomorphs in many *H. sinensis* strains and
843 proposed a facultative hybridization hypothesis for *O. sinensis*. Li et al. [37] analyzed transcriptome
844 assemblies of *H. sinensis* strains focusing on the mating-type genes of *MAT1-1* and *MAT1-2* idiomorphs
845 and reported the differential transcription of mating-type genes in Genotype #1 *H. sinensis* strains, in
846 addition to the differential occurrence of the mating-type genes in 237 *H. sinensis* strains.

847 Liu et al. [78] reported that the MAT1-1-1 gene was absent, but the MAT1-2-1 gene was present in
848 the transcriptome assembly GCQL00000000 of the *H. sinensis* Strain L0106. Although Bushley et al. [60]
849 reported the detection of transcripts of mating-type genes of both *MAT1-1* and *MAT1-2* idiomorphs in *H.*
850 *sinensis* Strain 1229, the MAT1-2-1 transcript contained nonspliced intron I that contains 3 stop codons.
851 This transcript would then produce a largely truncated MAT1-2-1 protein, lacking the major portion of the
852 protein encoded by exons II and III [37], inevitably resulting in biological dysfunction of the truncated
853 MAT1-2-1 protein. Thus, the evidence of the differential transcription of mating-type genes indicated the
854 self-sterilization of Genotype #1 *H. sinensis* and the inability to carry out self-fertilization under
855 homothallic or pseudohomothallic reproduction [47,60].

856 The evidence of genetic, transcriptional and coupled transcriptional-translational controls indicated
857 the requirement of sexual partners of *O. sinensis* to carry out sexual reproduction in the lifecycle of natural

858 *C. sinensis*. The potential sexual partners in physiological heterothallism may be coexisting intraspecific
859 GC-biased Genotypes #1 of *O. sinensis*, monoecious or dioecious [8–10,15,37]. For instance, *H. sinensis*
860 Strains 1229 and L0106 may be able to produce complementary mating proteins and potentially act as
861 sexual partners in physiological heterothallic reproduction [10,37,47,78].

862 The potential sexual partners may also be heterospecific fungal species cocolonized in natural and
863 cultivated *C. sinensis* if the fungi are able to break through the interspecific reproductive isolation barrier
864 to achieve hybridization. Notably, the taxonomic positions of GC-biased Genotypes #2–3 and #7–14 and
865 AT-biased Genotypes #4–6 and #15–17 have not been determined, probably due to their *H. sinensis*-like
866 morphological and growth characteristics and nonculturability *in vitro* leading to technical difficulties in
867 fungal isolation and purification [8–10,29,57,65,67]. However, they most likely belong to independent *O.*
868 *sinensis* fungi because their sequences do not reside in the genome of Genotype #1 *H. sinensis* [8–
869 10,47,51–54,67] and because of the phylogenetic analysis and conclusion by Stensrud et al. [65] that a
870 large sequence variation in the conservative 5.8S gene "far exceeds what is normally observed in fungi …
871 even at higher taxonomic levels (genera and family)." Studies have reported a close association of GC-
872 biased Genotypes #1 and #2 and AT-biased genotypes of *O. sinensis* differentially with dynamic genotypic
873 alterations in the compartments of natural *C. sinensis*, especially in the teleomorphic SFPs and ascospores
874 in the sexual life stages presented in this study and other studies [8–10,15–16,19–21,37,61]. Hopefully,
875 the multiple genotypes of *O. sinensis* reported in this study and the companion study [61] may potentially
876 serve as sexual partners for hybridization if they are finally determined to be independent fungal species.
877 Coincidentally, transcriptome assemblies of *H. sinensis* Strain L0106 and *S. hepiali* Strain Feng showed
878 differential transcription of mating-type genes that were complementary to each other [37,78–79].

879 These findings provide genetic and transcriptomic evidence for the possible outcrossing of *O. sinensis*
880 fungi and encourage further investigation of their reproductive physiology. In addition, Li et al.
881 [10,37,61,67] provided evidence of the potential hybridization or parasexual reproduction of Group-A *H.*
882 *sinensis* and an AB067719-type Group-E fungus in *C. sinensis* ascospores, producing genetically variant
883 offspring (Genotypes #13–14 of *O. sinensis*). The evidence of complex reproduction behaviors of *O.*
884 *sinensis* supports the facultative hybridization hypothesis for *O. sinensis* proposed by Zhang & Zhang
885 [77].

886

887 ## Uncertain anamorph-teleomorph connection in *O. sinensis*

888 This paper presented herein and its companion paper [61] demonstrated multiple GC- and AT-biased
889 genotypic teleomorphs of *O. sinensis* in the compartments of natural *C. sinensis*. Our findings question
890 the anamorph-teleomorph connection in *O. sinensis*, which has been the subject of a decades-long
891 academic debate [6–10,26,40,67]. Wei et al. [39] attempted to conclude this debate with the sole anamorph
892 hypothesis for *H. sinensis* based on the aforementioned 3 lines of evidence that satisfy the requirements
893 of the first and second criteria of Koch's postulates but not the third and fourth criteria, thus leaving the
894 hypothesis uncertain, although the hypothesis has been widely appreciated.

895 To supplement the evidence, Wei et al. [46] reported a successful industrial artificial cultivation
896 project to meet the third criterion of Koch's postulates, reportedly using GC-biased Genotype #1 *H.*
897 *sinensis* Strains 130508-KD-2B, 20110514, and H01-20140924-03 as inoculants. They reported the
898 production of fruiting bodies of cultivated *C. sinensis* under product-orientated industrial settings, which
899 are distinct from the extreme strictness under research-orientated academic settings. With keeping some
900 critical technical information as a trade secret, the authors identified a sole teleomorph of *O. sinensis* in
901 the fruiting body of cultivated *C. sinensis* belonging to AT-biased Genotype #4 of *O. sinensis*. Thus, the
902 species mismatching between the anamorphic inoculants and the sole-teleomorph in the final cultivated
903 products failed to meet the requirement of the fourth criterion of Koch's postulates because the sequence
904 of AT-biased Genotype #4 does not reside in the genomes of GC-biased Genotype #1 *H. sinensis* Strains
905 1229, CC1406-203, Co18, IOZ07 and ZJB12195 [6–10,47–54,67]. In addition to teleomorphic AT-biased
906 Genotype #4 of *O. sinensis* found in cultivated *C. sinensis*, Wei et al. [46] also reported teleomorphic GC-
907 biased Genotype #1 in natural *C. sinensis*. These results presented by Wei et al. [46] invalidated the
908 hypotheses of a sole anamorph for *H. sinensis* and a sole teleomorph of Genotype #1 of *O. sinensis*
909 proposed 10 years ago by the same group of key authors [39].

910 To support the sole anamorph and sole teleomorph hypotheses for Genotype #1 of *O. sinensis* [39],
911 Li et al. [59] proposed that all AT-biased genotypes are "ITS pseudogene" components "in a single
912 genome" of Genotype #1 *H. sinensis*. Li et al. [80] further proposed that all pseudogenic AT-biased
913 genotypes were generated through RIP (repeat-induced point mutation) mutagenesis and "could have
914 emerged either before or after a new functional (*i.e.*, GC-biased) ITS haplotype was generated (by random
915 mutation)" and co-occurred "in a single genome" of Genotype #1 of *O. sinensis*. In addition to the genome
916 residency test demonstrating that the sequences of mutant Genotypes #2–17 are absent from the genome

917 of Genotype #1 *H. sinensis*, we analyzed multiple repetitive ITS copies in the genome assemblies
918 JAAVMX000000000 and NGJJ00000000 of Genotype #1 *H. sinensis* Strains IOZ07 and CC1406-203,
919 respectively (*cf.* Fig 2) [51,53]. The multiple repetitive ITS copies in the genomes feature multiple
920 scattered insertion/deletion and transversion point mutations, which might not be induced through RIP
921 mutagenesis that theoretically causes cytosine-to-thymine (C-to-T) and guanine-to-adenine (G-to-A)
922 transition mutations. The phylogenetic analysis shown in Fig 2 (the topology of the phylogenetic tree was
923 confirmed by Bayesian majority rule consensus phylogenetic analyses [10,61,65–67]) demonstrated that
924 all sequences of repetitive ITS copies in JAAVMX000000000 and NGJJ00000000 were clustered into the
925 GC-biased genotype clade along with GC-biased genotypes, far distant from the AT-biased genotype
926 clade. The transition mutant AT-biased genotypes might indeed be induced through RIP mutagenesis (or
927 through other mutagenic mechanisms) from a common evolutionary ancestor in the long history of
928 evolution [65] and formed independent evolutionary offspring *O. sinensis* fungi [10,13,61,65,67]. There
929 has been no evidence thus far to prove that AT-biased genotypes with multiple scattered transition alleles
930 (*cf.* Fig 1) emerged after a new GC-biased "ITS haplotype was generated" and co-occurred "in a single
931 genome" of Genotype #1 of *O. sinensis*, as hypothesized by Li et al. [80].

932 Other studies also provided evidence not consistent with the hypotheses of a sole anamorph for *H.*
933 *sinensis* and a sole teleomorph of *O. sinensis* Genotype #1. Barseghyan et al. [70] proposed a dual-
934 anamorph hypothesis for *O. sinensis* involving *H. sinensis* and *Tolypocladium sinensis* using macro- and
935 micromycological approaches, unfortunately without molecularly genotyping the *O. sinensis* fungus
936 showing *H. sinensis*-like morphological and growth characteristics. Engh [27] hypothesized that *C.*
937 *sinensis* and *T. sinensis* form a fungal complex. A *C. sinensis* sequence (AJ786590) that was discovered
938 by Engh [27] and disclosed by Stensrud et al. [69] was 99.4% homologous to that of AT-biased Genotype
939 #4 AB067744 of *O. sinensis* [6–10,48–50,67]. Kinjo & Zang [29] and Mao et al. [57] reported the
940 detection of teleomorphic AT-biased Genotype #4 or #5 of *O. sinensis* in natural *C. sinensis* specimens
941 collected from geographically distant regions. Zhang et al. [55] and Cheng et al. [56] reported the detection
942 of GC-biased Genotype #3 of *O. sinensis* in the stroma of natural *C. sinensis* collected from Nyingchi in
943 Tibet. Chen et al. [58] reported the detection of GC-biased Genotype #7 of *O. sinensis* in the stroma of a
944 natural *C. sinensis* specimen collected from Qinghai Province. Mutant Genotypes #3–5 and #7 of *O.*
945 *sinensis* share the same *H. sinensis*-like morphological and growth characteristics, without the co-
946 occurrence of GC-biased Genotype #1 *H. sinensis* [6–10,27,29,55–58,69]. Microcycle conidiation studies
947 of *C. sinensis* ascospores showed conidia with *H. sinensis*-like morphological and growth characteristics,

948 but molecular genotyping was not performed [41–43]. Li et al. [59] identified both GC-biased Genotype
949 #1 and AT-biased Genotype #5 in 25-day cultures of teleomorphic monoascospores of *C. sinensis*,
950 exhibiting multicellular heterokaryons [60]. Li et al. [61] identified GC-biased Genotype #1, AT-biased
951 Genotypes #5–6 and #16, and Genotypes #13–14 of large DNA segment reciprocal substitutions and
952 genetic material recombination in teleomorphic ascospores of *C. sinensis*, which co-occurred with *S.*
953 *hepiali* and an AB067719-type fungus. The current study revealed the dynamic alterations of GC-biased
954 genotype and AT-biased Cluster-A genotypes in an asynchronous, disproportional manner in teleomorphic
955 ascospores of *C. sinensis* and additional AT-biased Cluster-B genotypes in the sexual organ SFPs (with
956 ascocarps) of natural *C. sinensis*. These studies demonstrated differential co-occurrence of multiple
957 teleomorphs of *O. sinensis*, nonsupportive to the sole anamorph and a sole teleomorph hypothesis [39].

958

959

960 # Conclusions

961 Multiple teleomorphic genotypes of *O. sinensis* co-occur in different combinations with dynamic
962 alterations in the SFPs (densely covered with numerous ascocarps) and ascospores of natural *C. sinensis*,
963 demonstrating their genomic independence and thus providing evidence that they belong to independent
964 fungi. Metagenome members, including several genotypes of *O. sinensis*, play symbiotic roles in different
965 developmental and maturational stages in different compartments of natural *C. sinensis* to achieve sexual
966 reproduction of *O. sinensis* during the lifecycle of natural *C. sinensis*.

967

968

969 # Acknowledgments

970 The authors are grateful to Prof. Mu Zang, Prof. Zong-Qi Liang, Prof. Ru-Qin Dai, Prof. Ying-Lan
971 Guo, Prof. Ping Zhu, Prof. Zhao-Lan Li, Prof. Yu-Guo Zheng, Dr. Jia-Gang Zhao and Dr. Yan-Jiao Zhou
972 for consultations, and Prof. Xin Liu, Prof. Hai-Feng Xu, Ms. Xiao-Li Ma, Ms. Ming Yang, Mr. Zong-Hao
973 Zhang, Mr. Wei Chen, Mr. Tao-Ye Zheng, Mr. Jin-Jin Li, and Mr. Yu-Chun Zhou for their assistance.

974

975

976 **[REFERENCES]**

977 [1] Song L-R, Hong X, Ding X-L, Zang Z-Y. *Monographs of Modern Pharmacy of Chinese*
978 *Traditional Medicine*. People′s Health Publishing House, Beijing 2001. pp. 733–737.

979 [2] Zhu J-S, Halpern GM, Jones K. The scientific rediscovery of a precious ancient Chinese herbal
980 regimen: *Cordyceps sinensis*: Part I. J. Altern. Complem. Med. 1998a;4(3): 289–303.

981 [3] Zhu J-S, Halpern GM, Jones K. The scientific rediscovery of an ancient Chinese herbal medicine:
982 *Cordyceps sinensis*: Part II. J. Altern. Complem. Med. 1998b;4(4): 429–457.

983 [4] Li C-L, Tan N-Z, Berger JL, Ferguson SB, Zhang Y, Prolla TA, et al. The Combined use of
984 ageLOC whole-gene expression profiling technology and mouse lifespan test in anti-aging herbal
985 product study. Proc. 2011 New TCM Prod. Innovat. Indust. Devel. Summit, Hangzhou, China,
986 2011, pp. 443–448

987 [5] Tan N-Z, Berger JL, Zhang Y, Pr TA, Weindruch R, Zhao C-S, et al. The lifespan-prolonging effect
988 of *Cordyceps sinensis* Cs-4 in normal mice and its molecular mechanisms. FASEB J. 2011;25(1):
989 599.1

990 [6] Yao Y-S, Zhu J-S. Indiscriminative use of the Latin name for natural *Cordyceps sinensis* insect-
991 fungi complex and multiple *Ophiocordyceps sinensis* fungi. Chin. J. Chin. Mater Med. 2016;41(7):
992 1361–1366.

993 [7] Zhu J-S, Wu J-Y. Genetic heterogeneity of natural *Cordyceps sinensis* with co-existence of
994 multiple fungi. Chin. J. Cell Biol. 2015;37(2): 284–298.

995 [8] Li Y-L, Yao Y-S, Xie W-D, Zhu J-S. Molecular heterogeneity of natural *Cordyceps sinensis* with
996 multiple *Ophiocordyceps sinensis* fungi challenges the anamorph-teleomorph connection
997 hypotheses and implementation of the Amsterdam Declaration of IMA. Am. J. Biomed. Sci.
998 2016;8(2): 123−159.

999 [9] Zhu J-S, Li Y-L. A Precious Transitional Chinese Medicine, *Cordyceps sinensis*: Multiple
1000 heterogeneous *Ophiocordyceps sinensis* in the insect-fungi complex. Lambert Academic
1001 Publishing, Saarbrüchen. Germany 2017.

1002 [10] Li Y-L, Li X-Z, Zhu J-S. *Cordyceps sinensis* Fungal Heterokaryons. Chemistry Industry Press Co.,
1003 Beijing, China, 2022.

1004 [11] Liu Y-N, Jin Y-S, Liu Z, Han Y-N. *Cordyceps sinensis* cDNA library construction and
1005 identification. Chin. J. Informat. TCM 2006;13(9): 43−45.

1006 [12] Yang J-L, Xiao W, He H-H, Zhu H-X, Wang S-F, Cheng K-D, et al. Molecular phylogenetic
1007 analysis of *Paecilomyces hepiali* and *Cordyceps sinensis*. Acta Pharmaceut. Sinica. 2008;43(4):
1008 421–426.

1009 [13] Xiao W, Yang J-P, Zhu P, Cheng K-D, He H-X, Zhu H-X, et al. Non-support of species complex
1010 hypothesis of *Cordyceps sinensis* by targeted rDNA-ITS sequence analysis. Mycosystema.
1011 2009;28(6): 724–730.

1012 [14] Zhu J-S, Guo Y-L, Yao Y-S, Zhou Y-J, Lu J-H, Qi Y, et al. Maturation of *Cordyceps sinensis*
1013 associates with co-existence of *Hirsutella sinensis* and *Paecilomyces hepiali* DNA and dynamic
1014 changes in fungal competitive proliferation predominance and chemical profiles. J. Fungal Res.
1015 2007;5(4): 214–224.

1016 [15] Zhu J-S, Gao L, Li X-H, Yao Y-S, Zhou Y-J, Zhao J-Q, et al. Maturational alterations of oppositely
1017 orientated rDNA and differential proliferations of CG:AT-biased genotypes of *Cordyceps sinensis*
1018 fungi and *Paecilomyces hepiali* in natural *C. sinensis*. Am. J. Biomed. Sci. 2010;2(3): 217–238.

1019 [16] Zhu J-S, Zhao J-G, Gao L, Li X-H, Zhao J-Q, Lu J-H. Dynamically altered expressions of at least
1020 6 *Ophiocordyceps sinensis* mutants in the stroma of *Cordyceps sinensis*. J. Fungal Res.
1021 2012;10(2): 100–112.

1022 [17] Xiao Y-Y, Cao Y-M, Zhang L, Li C-R. Study on Genetic Diversity of Anamorphic Isolates from
1023 Different Sources of *Ophiocordyceps sinensis* by ISSR. J. Fungal Res. 2014;12(3): 154–159.

1024 [18] Liang Z-Q, Han Y-F, Liang J-D, Dong X, Du W. Issues of concern in the studies of
1025 *Ophiocordyceps sinensis*. Microbiol. Chin. 2010;37(11): 1692–1697.

1026 [19] Gao L, Li X-H, Zhao J-Q, Lu J-H, Zhu J-S. Detection of multiple *Ophiocordyceps sinensis*
1027 mutants in premature stroma of *Cordyceps sinensis* by MassARRAY SNP MALDI-TOF mass
1028 spectrum genotyping. J. Peking Univ. (Health Sci.). 2011;43(2): 259–266.

1029 [20] Gao L, Li X-H, Zhao J-Q, Lu J-H, Zhao J-G, Zhu J-S. Maturation of *Cordyceps sinensis* associates
1030 with alterations of fungal expressions of multiple *Ophiocordyceps sinensis* mutants with transition
1031 and transversion point mutations in stroma of *Cordyceps sinensis*. J. Peking Univ. (Health Sci.).
1032 2012;44(3): 454–463.

1033 [21] Yao Y-S, Zhou Y-J, Gao L, Lu J-H, Zhu J-S. Dynamic alterations of the differential fungal
1034 expressions of *Ophiocordyceps sinensis* and its mutant genotypes in stroma and caterpillar during
1035 maturation of natural *Cordyceps sinensis*. J. Fungal Res. 2011;9(1): 37–49,53.

1036 [22] Yao Y-S, Gao L, Li Y-L, Ma S-L, Wu Z-M, Tan N-Z, et al. Amplicon density-weighted algorithms
1037 analyze dissimilarity and dynamic alterations of RAPD polymorphisms in the integrated micro-
1038 ecosystem *Cordyceps sinensis*. J. Peking Univ. (Health Sci.). 2014;46(4): 618–628.

1039 [23] Dong Y-Z, Zhang L-J, Wu Z-M, Gao L, Yao Y-S, Tan N-Z, et al. Altered proteomic polymorphisms
1040 in the caterpillar body and stroma of natural *Cordyceps sinensis* during maturation. PLoS ONE.
1041 2014;9(10): e109083. doi: 10.1371/journal.pone.0109083

1042 [24] Ni L-Q, Yao Y-S, Gao L, Wu Z-M, Tan N-Z, Wu J-Y, et al. Density-weighted algorithms for
1043 similarity computation and cluster tree construction in the RAPD analysis of a micro-ecosystem
1044 *Cordyceps sinensis*. Am. J. Biomed. Sci. 2014;6(2): 82–104.

1045 [25] Zhang W-W, Cheng X-L, Liu X-Z, Xiang M-C. Genome Studies on Nematophagous and
1046 Entomogenous Fungi in China. J Fungi. 2016;2: 9. doi:10.3390/jof2010009

1047 [26] Jiang Y, Yao Y-J. A review for the debating studies on the anamorph of *Cordyceps sinensis*.
1048 Mycosistema. 2003;22(1): 161–176.

1049 [27] Engh IB. Molecular phylogeny of the *Cordyceps-Tolypocladium* complex. Candidate scientific
1050 thesis, Department of Biology, University of Oslo, 1999.

1051 [28] Zhao J, Wang N, Chen Y-Q, Li T-H, Qu L-H. Molecular identification for the asexual stage of
1052 *Cordyceps sinensis*. Acta Sci. Nat. Univ. Sunyatseni. 1999;38(1): 122–123.

1053 [29] Kinjo N, Zang M. Morphological and phylogenetic studies on *Cordyceps sinensis* distributed in
1054 southwestern China. Mycoscience. 2001;42: 567–574.

1055 [30] Chen Y-Q, Wang N, Li T-H, Zhang W-M. Determination of the anamorph of *Cordyceps sinensis*
1056 inferred from the analysis of the ribosomal DNA internal transcribed spacers and 5.8S rDNA.
1057 Biochem. Syst. Ecol. 2001;29: 597–607.

1058 [31] Chen Y-Q, Hu B, Xu F, Zhang W-M, Zhou H, Qu L-H. Genetic variation of *Cordyceps sinensis*, a
1059 fruit-body-producing entomopathegenic species from different geographical regions in China.
1060 FEMS Microbiol. Lett. 2004;230: 153–158.

1061 [32] Liu Z-Y, Yao Y-J, Liang Z-Q, Liu A-Y, Pegler DN, Chase M-W. Molecular evidence for the
1062 anamorph-teleomorph connection in *Cordyceps sinensis*. Mycol. Res. 2001;105(7): 827–832.

1063 [33] He S-Q, Jin X-L, Luo J-C, Wang C-M, Wang S-R. Morphological characteristics and submerged
1064 culture medium screening of a strain of *Geomyces pannorum* isolation from *Cordyceps sinensis*.
1065 Chin. J. Grassland. 2010;32(z1): 70–75.

1066 [34] He S-Q, Jin X-L, Luo J-C, Wang C-M. Morphological characteristics and submerged culture
1067 medium screening of *Pseudogymnoascus roseus*. Microbiol. Chin. 2011;38(9): 1371−1376.

1068 [35] Zhang Y-J, Sun B-D, Zhang S, Wàngmǔ, Liu X-Z, Gong W-F. Mycobiotal investigation of natural
1069 *Ophiocordyceps sinensis* based on culture-dependent investigation. Mycosistema. 2010;29(4):
1070 518–527.

1071 [36] Xia F, Liu Y, Shen G-L, Guo L-X, Zhou X-W. Investigation and analysis of microbiological
1072 communities in natural *Ophiocordyceps sinensis*. Can. J. Microbiol. 2015;61: 104–111.

1073 [37] Li X-Z, Li Y-L, Zhu J-S. *Differential expression of mating-type genes in Hirsutella sinensis and*
1074 *natural Cordyceps sinensis*. Proc. 2021 Intl. Conf. Info. Technol. Biomed. Engineering, 2021, pp.
1075 318−333. https://conferences.computer.org/icitbepub/pdfs/ICITBE2021-
1076 6JNtJiThlp10s9N5Sodvuy/009900a318/009900a318.pdf

1077 [38] Yang J-Y, Tong X-X, He C-Y, Bai J, Wang F, Guo J-L. Comparison of endogenetic microbial
1078 community diversity between wild *Cordyceps sinensis*, artificial *C. sinensis* and habitat soil. Chin.
1079 J. Chin. Materia Medica. 2021;46(12): 3106–3115.

1080 [39] Wei X-L, Yin X-C, Guo Y-L, Shen N-Y, Wei, J.-C. Analyses of molecular systematics on
1081 *Cordyceps sinensis* and its related taxa. Mycosystema. 2006;25(2): 192–202.

1082 [40] Liang Z-Q. Anamorphs of *Cordyceps* and their determination. Southwest Chin. J. Agricult. Sci.
1083 1991;4(4): 1–8.

1084 [41] Mo M-H, Chi S-Q, Zhang K-Q. Microcycle conidiation of *Cordyceps sinensis* and anamorph
1085 isolation. Mycosystema. (2001;20: 482−485.

1086 [42] Liu Z-Y, Liang Z-Q, Liu A-Y. Investigation on microcycle conidiation of ascospores and
1087 conidiogenous structures of anamorph of *Cordyceps sinensis*. Guizhou Agricult. Sci. 2003;31(1):
1088 3–5.

1089 [43] Xiao Y-Y, Chen C, Dong J-F, Li C-R, Fan M-Z. Morphological observation of ascospores of
1090 *Ophiocordyceps sinensis* and its anamorph in growth process. J. Anhui Agricult. Univ. 2011;38(4):
1091 587–591.

1092 [44] Wang N, Chen Y-Q, Zhang W-M, Li T-H, Qu L-H. Molecular evidence indicating multiple origins
1093 in the entomogenous *Cordyceps*. Acta Sci. Nat. Univ. Sunyatseni. 2000;39: 70−73.

1094 [45] Li Z-Z, Huang B, Li C-R, Fan M-Z. Molecular evidence for anamorph determination of *Cordyceps*
1095 *sinensis* (Berk.) Sacc. Mycosystema. 2000;9(1): 60–64.

1096 [46] Wei J-C, Wei X-L, Zheng W-F, Guo W, Liu R-D. Species identification and component detection
1097 of *Ophiocordyceps sinensis* cultivated by modern industry. Mycosystema. 2016;35(4): 404–410.

1098 [47] Hu X, Zhang Y-J, Xiao G-H, Zheng P, Xia Y-L, Zhang X-Y, St Leger RJ, Liu X-Z, Wang C-S.
1099 Genome survey uncovers the secrets of sex and lifestyle in caterpillar fungus. Chin. Sci. Bull.
1100 2013;58: 2846–2854.

1101 [48] Li X-Z, Li Y-L, Yao Y-S, Xie W-D, Zhu J-S. Further discussion with Li et al. (2013, 2019)
1102 regarding the "ITS pseudogene hypothesis" for *Ophiocordyceps sinensis*. Mol. Phylogenet. Evol.
1103 2020;146: 106728. https://doi.org/10.1016/j.ympev.2019.106728

1104 [49] Zhu J-S, Li Y-L, Yao Y-S, Xie W-D. Molecular evidence not supporting the use of *Hirsutella*
1105 *sinensis* strain EFCC7287 as the taxonomic standard for multiple *Ophiocordyceps sinensis* fungi.
1106 Intl. J. Mol. Biol. 2018;3: 114−115.

1107 [50] Zhu J-S, Li Y-L, Yao Y-S, Xie W-D. The multiple genotypes of *Ophiocordyceps sinensis* and the
1108 "ITS pseudogene" hypothesis. Mol. Phylogenet Evol. 2019;139: 106322. doi:
1109 10.1016/j.ympev.2018.10.034

1110 [51] Liu J, Guo L-N, Li Z-W, Zhou Z, Li Z, Li Q, et al. Genomic analyses reveal evolutionary and
1111 geologic context for the plateau fungus *Ophiocordyceps sinensis*. Clin. Med. 2020;15: 107–119.

1112 [52] Jin L-Q, Xu Z-W, Zhang B, Yi M, Weng C-Y, Lin S, et al. Genome sequencing and analysis of
1113 fungus *Hirsutella sinensis* isolated from *Ophiocordyceps sinensis*. AMB Expr. 2020;10: 105.
1114 https://doi.org/10.1186/s13568-020-01039-x

1115 [53] Shu R-H, Zhang J-H, Meng Q, Zhang H, Zhou G-L, Li M-M, et al. A new high-quality draft
1116 genome assembly of the Chinese cordyceps *Ophiocordyceps sinensis*. Genome Biol. Evol.

1117 2020;12(7): 1074−1079.

1118 [54] Li Y, Hsiang T, Yang R-H, Hu X-D, Wang K, Wang W-J, et al. Comparison of different sequencing
1119 and assembly strategies for a repeat-rich fungal genome, *Ophiocordyceps sinensis*. J. Microbiol.
1120 Methods. 2016;128: 1−6.

1121 [55] Zhang Y-J, Xu L-L, Zhang S, Liu X-Z, An Z-Q, Wàngmǔ, et al. Genetic diversity of
1122 *Ophiocordyceps sinensis*, a medicinal fungus endemic to the Tibetan Plateau: implications for its
1123 evolution and conservation. BMC Evol. Biol. 2009;9: 290. doi:10.1186/1471-2148-9-290

1124 [56] Cheng Q-Q, Cheng C-S, Ouyang Y, Lao C-C, Cui H, Xian Y, et al. Discovery of differential
1125 sequences for improving breeding and yield of cultivated *Ophiocordyceps sinensis* through ITS
1126 sequencing and phylogenetic analysis. Chin. J. Nat. Med. 2018;16(10): 0749−0755.

1127 [57] Mao X-M, Zhao S-M, Cao L, Yan X, Han R-C. The morphology observation of *Ophiocordyceps*
1128 *sinensis* from different origins. J Environ. Entomol. 2013;35(3): 343–353.

1129 [58] Chen C-S, Hseu R-S, Huang C-T. Quality control of *Cordyceps sinensis* teleomorph, anamorph,
1130 and Its products. Chapter 12, *in* (Shoyama, Y., Ed.) *Quality Control of Herbal Medicines and*
1131 *Related Areas*. InTech, Rijeka, Croatia, 2011. www.intechopen.com

1132 [59] Li Y, Jiao L, Yao Y-J. Non-concerted ITS evolution in fungi, as revealed from the important
1133 medicinal fungus *Ophiocordyceps sinensis*. Mol. Phylogenet. Evol. 2013;68: 373−379.

1134 [60] Bushley KE, Li Y, Wang W-J, Wang X-L, Jiao L, Spatafora JW, et al. Isolation of the MAT1-1
1135 mating type idiomorph and evidence for selfing in the Chinese medicinal fungus *Ophiocordyceps*
1136 *sinensis*. Fungal Biol. 2013;117(9): 599−610.

1137 [61] Li Y-L, Li X-Z, Yao Y-S, Wu Z-M, Lou Z-Q, Xie W-D, et al. Differential cooccurrence of multiple
1138 genotypes of *Ophiocordyceps sinensis* in the stromata, stromal fertile portion (ascocarps) and
1139 ascospores of natural *Cordyceps sinensis*. PLOS ONE. 2022. (submitted as a companion paper)

1140 BIORXIV Preprint 2022-9-19. https://www.biorxiv.org/content/10.1101/2022.06.20.496766v2.full.pdf

1141 [62] Li Y-L. Preliminary study on the ascospores of *Cordyceps sinensis*. Edible Fungi Chin.
1142 2002;21(4): 9−10.

1143 [63] Lin W-C, Wu Y-W, Xie M-C, Zhu J-S. Reduced liver necrosis and fibrosis and improved liver
1144 functions in a CCl4-induced hepatitis model by ReishiMax supplementation. Gastroenterol.

1145 2004;126(4II): A431.

1146 [64] Tamura K, Stecher G, Peterson D, Filipski A, Kumar S. MEGA6: Molecular Evolutionary
1147 Genetics Analysis version 6.0. Molecular Biology Evolution 2013;30: 2725−2729.

1148 [65] Stensrud Ø, Schumacher T, Shalchian-Tabrizi K, Svegardenib IB, Kauserud H. Accelerated
1149 nrDNA evolution and profound AT bias in the medicinal fungus *Cordyceps sinensis*. Mycol. Res.
1150 2007;111: 409–415.

1151 [66] Huelsenbeck JP, Ronquist F. MRBAYES: Bayesian inference of phylogeny. Bioinformat. 2001;17:
1152 754−755.

1153 [67] Li X-Z, Li Y-L, Yao Y-S, Xie W-D, Zhu J-S. Molecular identification of *Ophiocordyceps sinensis*
1154 genotypes and the indiscriminate use of the Latin name for the multiple genotypes and the natural
1155 insect-fungi complex. Am J BioMed Sci. 2022;14(3): 115−135.

1156 [68] Buetow KH, Edmonson M, MacDonald R, Clifford R, Yip P, Kelley J, et al. High-throughput
1157 development and characterization of a genome wide collection of gene-based single nucleotide
1158 polymorphism markers by chip-based matrix-assisted laser desorption/ionization time-of-flight
1159 mass spectrometry. Proc. Natl. Acad. Sci. USA. 2001;98(2): 581–584.

1160 [69] Stensrud Ø, Hywel-Jones NL, Schumacher T. Toward a phylogenetic classification of *Cordyceps*:
1161 ITS nrDNA sequence data confirm divergent lineages and paraphyly. Mycol. Res. 2005;109:
1162 41−56.

1163 [70] Barseghyan GS, Holliday JC, Price TC, Madison LM, Wasser SP. Growth and cultural-
1164 morphological characteristics of vegetative mycelia of medicinal caterpillar fungus
1165 *Ophiocordyceps sinensis* G.H. Sung et al. (Ascomycetes) Isolates from Tibetan Plateau
1166 (P.R.China). Intl. J. Med. Mushrooms. 2011;13(6): 565−581.

1167 [71] Zhang S, Zhang Y-J, Shrestha B, Xu J-P, Wang C-S, et al. *Ophiocordyceps sinensis* and *Cordyceps*
1168 *militaris*: research advances, issues and perspectives. Mycosystema. 2013;32: 577−597.

1169 [72] Li Y-L, Yao Y-S, Zhang Z-H, Xu H-F, Liu X, Ma S-L, et al. Synergy of fungal complexes isolated
1170 from the intestines of *Hepialus lagii* larvae in increasing infection potency. J. Fungal Res.
1171 2016;14: 96−112.

1172 [73] Wang Y-B, Wang Y, Fan Q, Duan D-E, Zhang G-D, Dai R-Q, et al. Multigene phylogeny of the

1173 family *Cordycipitaceae* (Hypocreales): new taxa and the new systematic position of the Chinese
1174 cordycipitoid fungus *Paecilomyces hepiali*. Fungal Diversity. 2020;103: 1–46.

1175 [74] Debuchy R, Turgeon BG. Mating-Type Structure, Evolution, and Function in Euascomycetes. In
1176 (eds. Kües U. & Fischer, R.) Growth, Differentiation and Sexuality. Springer, 2006. pp. 293–323.

1177 [75] Jones SK, Bennett RJ. Fungal mating pheromones: choreographing the dating game. Fungal Genet
1178 Biol. 2011;48(7): 668–676.

1179 [76] Wilson AM, Wilken PM, van der Nest MA, Steenkamp ET, Wingfield MJ, Wingfield BD.
1180 Homothallism: an umbrella term for describing diverse sexual behaviours. IMA Fungus 2015;6(1):
1181 207–214.

1182 [77] Zhang, S.; Zhang, Y.-J. Molecular evolution of three protein-coding genes in the Chinese
1183 caterpillar fungus *Ophiocordyceps sinensis*. Microbiol. China. 2015;42(8): 1549−1560.

1184 [78] Liu Z-Q, Lin S, Baker PJ, Wu L-F, Wang X-R, Wu H, Xu F, et al. Transcriptome sequencing and
1185 analysis of the entomopathogenic fungus *Hirsutella sinensis* isolated from *Ophiocordyceps*
1186 *sinensis*. BMC Genomics. 2015;16: 106–123.

1187 [79] Pang F, Wang L-P, Jin Y, Guo L-P, Song L-P, Liu G-M, et al. Transcriptome analysis of
1188 *Paecilomyces hepiali* at different growth stages and culture additives to reveal putative genes in
1189 cordycepin biosynthesis. Genomics 2018;110: 162–170.

1190 [80] Li Y, Jiang L, Wang K, Wu H-J, Yang R-H, Yan Y-J, Bushley KE, Hawksworth DL, Wu Z-J, Yao
1191 Y-J. RIP mutated ITS genes in populations of *Ophiocordyceps sinensis* and their implications for
1192 molecular systematics. IMA Fungus 2020;11: 18. https://doi.org/10.1186/s43008-020-00040-0

1193